Behaviour of alkali-activated concrete at elevated temperatures: A critical review

Wenlin Tu, Mingzhong Zhang [*]

Department of Civil, Environmental and Geomatic Engineering, University College London, London, WC1E 6BT, UK

A B S T R A C T

Alkali-activated concrete (AAC) is recognised as a novel sustainable construction material to substitute Portland cement concrete with superior thermal and mechanical performance. However, AAC would suffer significant deterioration when subjected to elevated temperatures due to different damage mechanisms, including thermal incompatibility caused by different thermal coefficients between matrix and aggregates, pore pressure build-up and phase transformation. This paper presents a systematic and comprehensive review on the behaviour of different types of AAC such as alkali-activated fly ash, alkali-activated slag, alkali-activated metakaolin and alkali-activated fly ash-slag systems at elevated temperatures in terms of phase stability and microstructural evolution as well as thermal and mechanical performance. The effective strategies for improving the high-temperature resistance of AAC are reviewed and discussed from the perspectives of AAC matrix, aggregates and fibre incorporation, with special focus on how these strategies can tackle different damage mechanisms. This paper summarises the recent advances in the field and identifies the remaining challenges and opportunities for future research.

1. Introduction

When concrete is subjected to elevated temperatures, the damage will be induced with development of cracks which can cause serious risks or even catastrophes if any large-scale concrete structure collapses [1–3]. In recent years, the behaviour of conventional Portland cement concrete (PCC) at elevated temperatures has been extensively studied from microscopic characterisation to macroscopic performance with a variety of approaches proposed to improve thermal and fire resistance of PCC [2,4–6]. As a promising alternative to PCC, alkali-activated concrete (AAC) is a sustainable cement-free construction material produced through alkaline activation of aluminosilicates such as fly ash and ground granulated blast-furnace slag, which can result in 60–80% less CO_2 emissions compared to PCC products [7–13]. The application of AAC as a substitute for PCC can not only help mitigate the CO_2 emissions from cement production, but also reduce the amount of industrial wastes, e.g., fly ash [14–17]. Moreover, AAC exhibits better mechanical performance and stable structure integrity at elevated temperatures of up to 800–900 °C in comparison with PCC [18,19]. Hence, the application of AAC in high temperature scenarios has been increasingly explored, such as fire-resistant materials, thermal insulators and thermal

energy storage concrete [20–23]. Nevertheless, AAC would also experience significant damage when exposed to high temperatures due to different mechanisms including thermal incompatibility, pore pressure build-up and phase transformation [24–26]. Thermal incompatibility is induced by the difference in thermal expansion coefficient of different constituents of AAC. For instance, aggregates tend to expand while AAC matrix experiences shrinkage when exposed to elevated temperatures, leading to crack initiation and propagation in AAC [25,27,28]. Pore pressure build-up results from the moisture transport from the heated surface to the cooler region in AAC matrix subjected to high temperatures and the accumulation of condensed water vapour in the non-deformable pore structure of AAC would cause damage and crack development [2,29,30]. Furthermore, the phase transformation and rearrangement of crystalline structure in AAC at elevated temperatures would lead to strength gain and loss, depending on the thermal stability [31–34]. Therefore, to promote the broader application of AAC in civil infrastructure, it is vital to systematically investigate the behaviour of AAC at elevated temperatures.

In recent years, an increasing number of studies have been focused on the behaviour of different types of AAC at elevated temperatures such as alkali-activated fly ash (AAF), alkali-activated slag (AAS), alkali-

---

* Corresponding author.
  E-mail address: mingzhong.zhang@ucl.ac.uk (M. Zhang).

activated metakaolin (AAMK) and alkali-activated fly ash-slag (AAFS) concrete. The experimental studies on AAF and AAS concrete indicated that AAF has superior mechanical performance against high temperatures due to the porous structure that can effectively prevent the vapour pressure build-up, while AAS exhibits the largest strength reduction in comparison with other types of AAC due to dehydration and decomposition of $CaCO_3$ [24–26]. Compared to AAF, AAMK has a denser internal structure and thus would suffer more serious deterioration in mechanical properties after exposure to 800 °C [35,36]. Regarding the blend precursor systems, e.g., AAFS, it was reported that the slag content has a significant influence on the thermal behaviour of AAFS in terms of microstructure and mechanical properties. AAFS containing low slag content (10–20% by weight of the binder) exhibits similar crystalline phases including quartz, mullite and nepheline to AAF but relatively better residual strength after exposure to high temperatures. The C–S–H type gel can be detected in both AAS and AAFS with high slag content (40–50% by weight), leading to a greater strength loss at elevated temperatures [33,37,38]. To tackle the potential risks of thermal-induced damage on concrete exposed to elevated temperatures, different mitigation approaches have been proposed and adopted. Among them, the addition of fibres such as steel, synthetic (e.g., polypropylene (PP)) and hybrid fibres is accepted as one of the most effective methods to enhance high-temperature resistance of cementitious materials and AAC [39]. For instance, the addition of steel fibres in concrete can resist the initiation and propagation of microcracks, while the incorporation of PP fibres can increase the connectivity of pore network in concrete and thus can effectively prevent the vapour pressure accumulation [40,41].

Up to now, several studies have summarised the behaviour of PCC at elevated temperatures and the performance of AAF and AAMK covering some thermal and mechanical properties at elevated temperatures from 25 °C to 1000 °C [1,3,19,39,42–46], while a critical review on the performance of different types of AAC subjected to high temperatures and damage mitigation approaches is still lacking. It is vital and urgent to summarise the recent advances in this field, which can provide a thorough understanding of the damage mechanisms of AAC exposed to elevated temperatures and promote the development of AAC with desired thermal and fire resistance for engineering application.

To this end, this study presents a state-of-the-art review and provides comprehensive discussions from microscopic characteristics to macroscopic performance of AAC at elevated temperatures. As illustrated in the outline of this review in Fig. 1, firstly, the heating and cooling methods and damage mechanisms of AAC in comparison with that of PCC were briefly introduced. Then, the microstructural characteristics and thermal and mechanical properties of different single and blend precursor systems subjected to elevated temperatures in terms of phase stability, microstructural evolution, thermal stability, thermal deformation, and compressive, tensile and flexural strengths were systematically reviewed and analysed. Afterwards, the potential approaches to mitigating damage of AAC at elevated temperatures including the modification of AAC and incorporation of fibres were summarised and discussed in detail. Lastly, the knowledge gap and remaining challenges were identified along with opportunities for future research.

2. Heating and cooling methods

The heating and cooling conditions have pronounced effects on the measurement of temperature-dependent properties of both PCC and AAC. In general, the thermal stress induced by temperature gradient in concrete is highly related to heating rate, which can significantly affect the mechanical performance of concrete after high temperature exposure [2,47]. Two main heating procedures are commonly employed: (1) simulation of the real fire situation following a standard heating curve, and (2) constant heating rate [1,40,48].

A standard heating rate is set based on the specified heating curves to predict the real fire conditions. Fig. 2a illustrates the standard fire curves
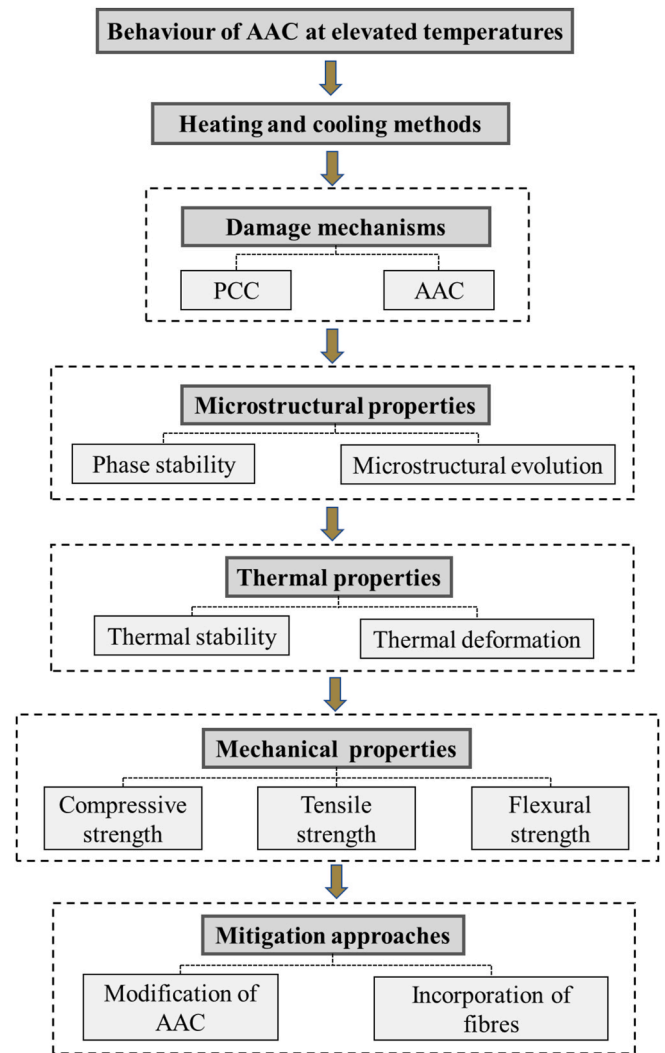

Fig. 1. Outline of this review.

given in ISO 834–1 [49], ASTM E119 [50], KSF 2257 [51] and JIS A 1304 [52], indicating a logarithmic relationship between the growing temperature and heating time to reflect the real fire circumstance [53–56]. This heating method has been extensively employed to investigate the resistance of concrete to pore pressure and spalling [1,57–60]. However, concrete can be significantly damaged by thermal gradient and thus structurally unstable with such a rapid increase of temperature in a short time period.

Therefore, the second method of increasing the temperature constantly at a relatively lower heating rate is applied to reach the target temperature more frequently [61–65]. Fig. 2b demonstrates the heating and cooling process of concrete with a fixed heating rate. A lower heating rate can minimise the thermal stress and isolate the effect of vapour pressure inside matrix. However, a slow heating rate may not completely prevent spalling of specimens due to the existence of pore pressure induced damage as a result of moisture vaporisation and pore pressure build-up [2]. The previous studies examined the heating rates between 0.5 and 30 °C/min such as 1 °C/min [2,65], 2 °C/min [66], 4 °C/min [67] and 10 °C/min [64,68,69]. Once the target temperature is attained at a constant speed, the temperature level is usually maintained for a certain period of time (1–2 h) to ensure that there is no temperature gradient inside the specimen while preventing the effect of long holding time on the mechanical properties of specimens [1].

The mechanical properties can be tested during and after heating process [41,63,70–78]. Due to the potential safety concerns on hot
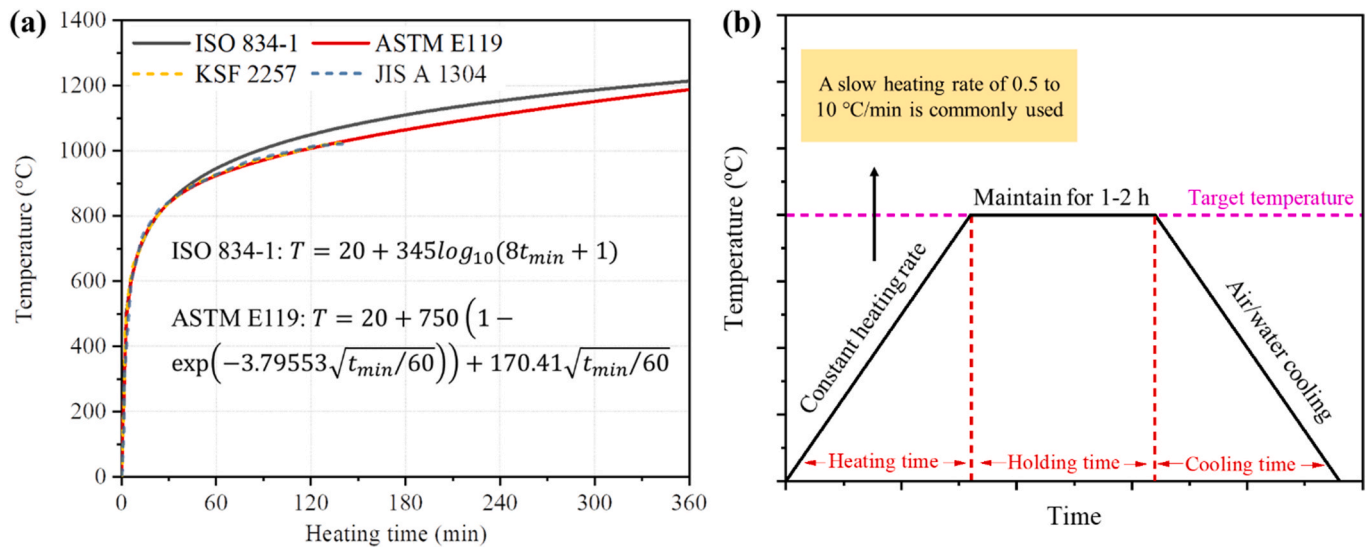
Fig. 2. Heating methods following (a) standard fire curves (T is the fire temperature and t_{min} is the heating time) and (b) constant heating process [1,55].

specimens, the tests are commonly conducted after heating. To measure the residual properties of specimens at ambient temperature, the test samples can be either cooled down instantly in water or naturally in furnace (air). It was reported that water cooling could cause 15.1% more deterioration in strength of the specimens than furnace cooling after exposure to 1100 °C, which can be attributed to the high heat transfer capacity of water with a rapid cooling process, leading to the generation of an unneglectable temperature gradient inside the concrete specimens [1,79]. Thus, the non-uniform distribution of thermal stress can cause damage to concrete and a strength loss.

It is worth noting that the measurement on specimens after cooling to room temperature may not fully represent the real situation for concrete structures in a fire circumstance [70,80]. Hot and residual compressive strengths of concrete specimens could be similar to each other [81,82]. However, it was also observed that there could be a large discrepancy between the temperature-dependent properties of concrete during exposure to elevated temperatures and after cooling [78,80,83]. At 100–105 °C, both the compressive and tensile strengths of hot specimens are much lower than those after cooling from the same temperature, which can be ascribed to the pore pressure-induced damage during heating [80,83]. At a higher temperature level of 600 °C, the strength of hot specimens suffers from inner tensile stresses induced by the thermal incompatibility between different phases (i.e., shrinkage of matrix and expansion of aggregates at elevated temperatures), which can further deteriorate the mechanical behaviour of specimens during exposure to high temperatures [78]. Due to the high facility requirements to undertake in-situ tests on hot specimens, the available data obtained from in-situ measurements are still limited. Table 1 summarises the recent experimental studies on ACC with different heating and cooling methods.

3. Damage mechanisms of concrete at elevated temperatures

3.1. Portland cement concrete (PCC)

The damage mechanism of PCC at elevated temperatures has been extensively studied. Fig. 3 displays a schematic illustration of pore pressure induced damage evolution in PCC at elevated temperatures. In general, up to 100 °C, the concrete specimen is fully in the moist zone with free-water evaporation. When the temperature continues to rise, the dehydration of hydration products in concrete takes place from the heated surface to the inner region. Afterwards, the decomposition of C–S–H gels starts and the chemically bounded water is released. As the

moisture flows towards the cold side of the concrete, the damage would occur with the initiation of cracks at the region with moisture accumulation [64,71,152–156]. It is widely accepted that the high-temperature induced damage of concrete can be mainly attributed to pore pressure build-up from trapped moisture inside matrix and thermal stress. Thus, three mechanisms were proposed to explain the damage evolution in PCC system, including pore pressure induced damage, thermal stress induced damage, and phase transformation.

The mechanism of pore pressure induced damage is associated with air and moisture migration in concrete. At elevated temperatures, moisture travels towards both directions of the heated surface and the inner matrix. Since the temperature is remained lower inside concrete, moisture can condense to form a "moisture clog". With the accumulation and expansion of condensed water vapour, a significant amount of potential energy is formed inside the pore network of concrete. Saturated vapour pressure, dilation of liquid water and partial pressure of enclosed air are all retained in the pores [157]. Consequently, the pore pressure builds up and the pore pressure induced stress would continue to increase until the maximum stress that can be maintained within the structure is exceeded, as a result of which damage would occur in concrete due to a violent release of energy.

However, pore pressure induced damage is not the only cause that leads to concrete failure [158]. The measured pore pressure can be relatively lower than tensile strength of concrete matrix, while the damage in concrete mainly results from the thermal stress induced by the temperature gradient inside concrete, i.e., the second mechanism [159,160]. In this case, the damage occurs due to concrete failure in compression at the heated surface. The exposed surface experiences not only compressive stresses but also tensile stresses from the inner parts due to restrained thermal expansion [157]. Thereby, the heating rate has a pronounced effect on the temperature gradient in concrete, which directly results in thermal stress induced damage. A higher heating rate tends to cause a greater temperature gradient.

From the previous studies on damage mechanisms of concrete at elevated temperatures, it is challenging to define the temperature-induced damage by a single factor, whereas the combined effect of both pore pressure and thermal stress induced damage is considered [161]. During heating, the thermal stress forms on the exposed surface, leading to the initiation of multi-cracks parallel to the heated surface, which are then filled and saturated with vapour pressure resulting in damage in concrete [157]. Furthermore, the heating rate can play a significant role in the damage mechanisms of concrete exposed to elevated temperatures. Following the standard fire heating rate, thermal

Table 1

Summary of raw materials, curing conditions, heating and cooling methods, characterisation and main findings collected from studies on AAC at elevated temperatures.

Ref.	Precursor	Alkaline activator	Additive	Fibre	Curing method	Heating method	Cooling method	Characterisation	Main findings
[27]	Fly ash	SH (8 and 14 M) + SS	–	–	24 h at 25, 40 and 80 °C oven curing, then ambient curing	Exposed to 100–1000 °C for 5 °C/min for 2 h	Naturally cool down	Compressive strength, mass loss, SEM, TGA	AAC surface had more deterioration due to temperature gradient. The strength loss after 600 °C can be ascribed to dehydration of reaction gels.
[31]	Fly ash	SH (10 M) + SS	–	–	24 h at 60 °C oven curing, then ambient curing	Exposed to 100–1200 °C for 2 h	Naturally cool down	Compressive and bond strengths, mass loss, TGA/DTG, XRD, SEM-EDS	The decrease of Si/Al ratio led to AAC strength loss. Class C fly ash caused denser microstructure and great mechanical performance after exposed to 800 °C.
[84]	Fly ash	SH + SS	–	–	24 h at 60 °C oven curing, then ambient curing	Exposed to up to 1200 °C in 5 min and hold for 2 h	Naturally cool down	Compressive and bond strengths, mass loss, TGA/DTG, XRD, SEM	No spalling occurred at 1200 °C. AAC exhibited better bond strength at 1200 °C compared to PCC. As the porous structure in AAC provided the channels for moisture to escape, with more stable crystalline phase.
[32]	Fly ash	SH (10 M) + SS	–	–	24 h at 75 °C oven curing, then ambient curing	Exposed to up to 200–800 °C at 5 °C/min and hold for 2 h	Naturally cool down	Compressive strength, mass loss, SEM, FTIR, XRD, TGA	The crystalline network in AAC was sensitive to the temperature increment. It kept stable at 600 °C, while the formation of new crystalline phases at 600–800 °C resulted in strength gain.
[85]	Fly ash	SH + SS	Bamboo ash (5–100%)	–	–	Exposed to 200–800 °C for 1 h	Air and water cooling	Compressive strength, mass loss, UPV	AAC with 100% fly ash showed 62% strength loss when exposed to 400–800 °C
[86]	Fly ash	SH (8 M) + SS	–	PVA and steel (both 0.75%)	24 h at 60 °C heat curing, then ambient curing	Exposed to 1000 °C at 5 °C/ min for 2 h	Air and water cooling	Tensile and compressive strengths	Water cooling can cause more obvious strength loss. Compared to PVA, the steel fibre reinforcement for AAC was more obvious.
[87]	Fly ash	SH + SS	–	–	24 h at 20 °C curing then ambient curing	Exposed to 100–800 °C at 2 °C/min for 1 h	Naturally cool down	Compressive strength, mass loss, SEM, TGA	The compressive strength increased up to 200 °C, due to secondary geopolymerisation between fly ash and alkaline activator but dropped after 200 °C due to dehydroxylation of N-A-S-H gel.
[88]	Fly ash	KOH (8 M) + K$_2$SiO$_3$	–	Carbon and basalt (0.5–1%)	24 h at 70 °C curing then ambient curing	Exposed to 200–800 °C at 5 °C/min	–	Compressive strength, mass loss, MIP, SEM	1% is the optimal dosage of carbon and basalt fibres for AAC. AAC containing carbon fibres showed less cracks at 600 °C and more compact microstructure than that with basalt fibres.
[89]	Fly ash	SH + SS	Micro silica (0–10%) granular filler	–	24 h at 80 °C curing then ambient curing	Exposed to 200–800 °C at 10 °C/min for 2 h	–	Compressive strength, thermal expansion and conductivity, XRD, TGA, FTIR, MAS-NMR analysis	5% is the optimal dosage of micro silica for fly ash-based AAC. Thermal conductivity of AAC decreased with the rise of temperature. Normal AAC exhibited around 2.5% thermal expansion.
[90]	Fly ash	SH (14 M) + SS	–	Rubber (10% by weight)	48 h at 90 °C curing then ambient curing	Exposed to 200–800 °C at 4.4 °C/min for 2 h	Naturally cool down	Compressive strength mass loss, XRD, TGA/DTG, FTIR	The compressive strength went up as the temperature increased from 600 to 800 °C. N-A-S-H was formed when increasing the temperature. Zeolite turned into nepheline and albite during the recrystallisation process at 600–800 °C.

Table 1 (*continued*)

Ref.	Precursor	Alkaline activator	Additive	Fibre	Curing method	Heating method	Cooling method	Characterisation	Main findings
[91]	Fly ash	SH (8 M) + SS KOH (8 M) + K$_2$SiO$_3$	Nano silica	–	24 h at 70 °C curing then ambient curing	Exposed to 200, 400, 600 and 800 °C	Naturally cool down	Mass loss, volume change, thermal shrinkage, XRD	Replacement of 10% of fly ash with fine silica can enhance thermal resistance of fly ash-based AAC.
[92]	Fly ash	SH + SS	–	Steel, PP	Ambient temperature curing	Exposed to 100, 200 and 300 °C	–	Compressive, splitting tensile, flexural strengths, flexural toughness	Fly ash-based AAC exhibited softening behaviour when subjected to elevated temperatures. The addition of fibres can improve the tensile strength and flexural toughness of AAC.
[93]	Fly ash	SH (10 M) + SS	–	–	24 h at 100 °C curing then ambient curing	Exposed to 200–800 °C at 5.5 °C/min for 1 h	Naturally cool down	Crack width, ductility, flexural behaviour	The load carrying capacity of AAC degraded rapidly when exposed to more than 600 °C.
[94]	Fly ash	SH + SS	–	–	48 h at 50–100 °C curing then ambient curing	Exposed to 200–800 °C at 7 °C/min	Naturally cool down	Compressive and flexural strengths, mass loss, UPV, SEM	Fly ash-based AAC had better compressive and flexural performance than that of PCC. After exposure to 800 °C, the compressive strength of AAC was improved from 7.63 MPa to 40.7 MPa.
[95]	Fly ash	SH (12 M) + SS	Light-weight fly ash aggregate	–	–	Exposed to 100–800 °C at 5 °C/min and held for 2 h	–	Elastic modulus, Compressive strength	There was a drop in strength when exposed to up to 200 °C, followed by a slight increase until 400 °C due to further geopolymerisation, and no strength loss occurred at 800 °C due to disintegration of reaction gels and phase transformation.
[96]	Fly ash	SH + SS	Quartz powder (0–30%)	–	24 h at 105 °C curing then ambient curing	Exposed to 400–1000 °C at 6.67 °C/min and held for 2 h	Naturally cool down	Compressive strength, workability, mass loss, XRD, SEM	The inclusion of quartz powder in fly ash and slag-based AAC improve thermal resistance due to the increase of Si/Al ratio.
[74]	Fly ash	SH (8 M) + SS KOH (8 M) + K$_2$SiO$_3$	–	Steel (0.5% and 0.75%)	24 h at 60 °C steam curing then 105 °C for 24 h	Exposed to 200–800 °C at 8 °C/min and held for 2 h	Naturally cool down	Elastic modulus, tensile and compressive strengths	Steel fibre reinforced AAC retained the compressive strength until 400 °C. AAC made from K-based activator had better tensile strength at elevated temperatures compared to that made from Na-based one.
[97]	Fly ash	SH + SS	–	–	72 h at 80 °C curing then ambient curing	Exposed to 200–1000 °C at 4.5 °C/min	Naturally cool down	Elastic modulus, Compressive strength, SEM	AAC retained around 60% of strength and stiffness when exposed to over 400 °C while fly ash particles was observed to collapse to form a homogeneous and compact structure when exceeding 600 °C.
[98]	Fly ash	SH (10–16 M) + SS	–	–	24 h at 105 °C curing then ambient curing	Exposed to 200–800 °C at 1 °C/min	–	Compressive strength, thermal expansion, physical appearance	The strength of AAC reduced when exposed to 400 °C but went up at 600–800 °C due to further geopolymerisation.
[99]	Fly ash	SH (14 M) + SS	–	–	24 h at 60 °C curing	Exposed to 400–1000 °C at ISO834 for 2.5 h	Naturally cool down	Compressive strength, mass loss, spalling	No spalling occurred in AAC. After exposed to 400 °C, the residual strength of AAC kept at around 93–107%.
[29]	Fly ash	SH + SS	–	Cotton fibres	–	Exposed to 200–1000 °C at 5 °C/min and held for 2 h	Naturally cool down	Compressive and flexural strengths, fracture toughness, TGA, SEM	The addition of cotton fibres can help inhibit crack development when AAC is subjected to elevated temperatures, owing to additional porosity and small channels.

Table 1 (*continued*)

Ref.	Precursor	Alkaline activator	Additive	Fibre	Curing method	Heating method	Cooling method	Characterisation	Main findings
[100]	Fly ash	SH + SS	–	–	72 h at 80 °C curing then ambient curing	4.5 °C/min	–	Compressive strength, thermal expansion, SEM	AAC experienced shrinkage induced by loss of moisture and densification of the matrix structure due to sintering effect.
[25]	Fly ash	SH (8 M) + SS	–	–	18 h at 60 °C curing then ambient curing	Exposed to 200–550 °C at 5 °C/min and held for 1 h	Naturally cool down	Elastic modulus, compressive strength, thermal strain, creep, TGA	As the temperature increased to 200–300 °C, the compressive strength of AAC increased due to further geopolymerisation.
[101]	Fly ash	SH + SS	Light-weight aggregate	–	24 h at 70 °C curing then ambient curing	Exposed to 400–800 °C at 4.4 °C/min and held for 1 h	Naturally cool down	Compressive strength, thermal expansion, TGA/DTG, XRD, SEM-EDS	The strength of AAC dropped after exposed to 400–600 °C due to dehydration and dehydroxylation. After exposed to 800 °C, the damage occurred due to sintering effect.
[102]	Fly ash	SH + SS	Light-weight aggregate	–	24 h at 70 °C curing then ambient curing	Exposed to 100–800 °C at 4.4 °C/min and held for 1 h	Naturally cool down	Compressive strength, thermal expansion, SEM	The residual strength of lightweight AAC increased when exposed to 100–300 °C, followed by a strength loss due to vapour effects and difference in thermal expansion between different phases in AAC.
[103]	Fly ash	SH + SS	–	–	24 h at 85 °C curing then ambient curing	Exposed to 300–900 °C at 8.5 °C/min and held for 2 h	Naturally cool down	Compressive strength, mass loss, shrinkage, water sorptivity, SEM-EDS, XRD	A rapid increase in volumetric strain of AAC happened when subjected to more than 600 °C. The sintering effect can be detected at elevated temperatures. The thermal performance of AAC with higher Si/Al ratio was better than that with lower Si/Al ratio.
[104]	Fly ash	SH + SS	–	–	18 h at 60 °C curing then ambient curing	Exposed to 100–680 °C at 5 °C/min and held for 1 h	Naturally cool down	Compressive strength, thermal strain, TGA	A glass transition point was detected in AAC with the increase of temperature to 560 °C. AAC exhibited brittle failure at any temperature level.
[28]	Fly ash	SH (7 M) + SS	–	–	24 h at 80 °C curing then ambient curing	Exposed to up to 800 °C at 4.4 °C/min and held for 1 h	Naturally cool down	Compressive strength, Thermal expansion, TGA/DTG	The residual strength of AAC at elevated temperatures was dependent on sample size. The thermal incompatibility was the dominant effect on the strength loss of AAC.
[24]	Fly ash	SH (10 M) + SS	–	–	24–96 h at 55–80 °C curing then ambient curing	Exposed to up to 800 °C at 4.4 °C/min and held for 2 h	Naturally cool down	Compressive strength, mass loss, TGA	Two opposing processes can affect the strength behaviour of AAC: (1) sintering effect to enhance strength, and (2) thermal incompatibility that deteriorates the matrix.
[105]	Fly ash	SH (7 M) + SS	–	–	24 h at 80 °C curing then ambient curing	Exposed to up to 800 °C at 5 °C/min and held for 1 h	Naturally cool down	Compressive strength, thermal expansion, TGA/DTG	Thermal incompatibility due to matrix shrinkage and aggregate expansion at elevated temperatures is the main cause for the strength loss of AAC.
[106]	Fly ash	SH + SS	–	–	24 h at 70 °C curing then ambient curing	Exposed to 100–1000 °C at 5 °C/min and held for 1 h	Naturally cool down	Compressive strength, mass loss, thermal expansion, SEM, XRD	Sintering can improve the interparticle bonding to enhance the residual strength of fly ash-based AAC at elevated temperatures while the strength loss was due to dehydration.

Table 1 (*continued*)

Ref.	Precursor	Alkaline activator	Additive	Fibre	Curing method	Heating method	Cooling method	Characterisation	Main findings
[107]	Fly ash	SH (10 M) +SS	–	–	Water curing	Fire heating to 500 and 1000 °C for 2 h	Naturally cool down	Compressive strength, Mass loss, FTIR, SEM	AAF exhibited higher fire resistance compared to PCC. Further geopolymerisation could lead to a denser microstructure in AAF.
[108]	Fly ash		–	Hybrid glass and basalt fibre	24 h at 80 °C curing then ambient curing	Exposed to 300–800 °C at 5 °C/min and held for 2 h	Naturally cool down	Flowability, compressive and flexural strengths, mass loss, SEM	Hybrid glass and basalt fibres could mitigate strength loss of AAF after high temperature exposure more efficiently compared to their single use. Glass fibres can provide bonding effect.
[109]	Fly ash	SH + SS	–	–	24 h at 85 °C curing then 23 °C water curing for 27 d	Exposed to 200–1000 °C at 4 °C/min and held for 1 h	Naturally cool down	Compressive strength Thermal diffusivity TGA, FTIR, XRD, SEM	Further geopolymerisation with an increase of N-A-S-H gel was detected after AAF was exposed to 200 °C. A phase transformation from amorphous to new crystalline phases took place after exposure to 600 °C.
[110]	Fly ash	SH + SS	–	–	24 h at 60 °C curing then 25 °C water curing for 28 d	Exposed to fire at 500 and 1200 °C and held for 2 h	–	Compressive strength, FTIR	A higher structural integrity was found in AAF compared to PCC. A more compact and denser internal structure was obtained in AAF matrix after high temperature exposure.
[111]	Fly ash	SH + SS	–	–	–	Exposed to 200–800 °C at 8 °C/min and held for 2 h	Naturally cool down	Compressive and flexural strengths, UPV, SEM	The inclusion of steel fibres enhanced thermal resistance of AAF in terms of physical and mechanical properties such as compressive and flexural strengths.
[112]	Slag	SH (10 M) + SS	0–100% recycled concrete aggregate	–	24 h at 80 °C curing then 23 °C water curing for 27 d	Exposed to 100–800 °C for 1 h	Air, oven and water cooling	Compression strength, mass loss, UPV, microstructures	The microstructure of ACC deteriorated with the increase of temperature and decrease of Ca/Si ratio while increase of Si/Al ratio. ITZ was weakened.
[113]	Slag	SH + SS	Calcined perlite (0, 25 and 50%)	–	48 h at 70 °C oven curing, then ambient curing	Exposed to 105 °C for 48 h, then 400–800 °C at 6 °C/min	Naturally cool down	Compressive and flexural strengths, mass loss, XRD, SEM-EDS	With the increase of temperature, the residual flexural and compressive strengths of AAS decreased and the mass loss of AAS increased.
[114]	Slag	SH (10 M) + SS	–	–	Ambient curing (29 °C)	Exposed to 200–1000 °C at 10 °C/min for 1 h	–	Compressive strength, mass loss, TGA/DTG, SEM, XRD, FTIR	Crack healing of AAC happened at 800–1000 °C. No spalling occurred at elevated temperatures. The compressive strength dropped by 90.6% at 800 °C due to decomposition but went up at 1000 °C due to rearrangement of crystalline.
[115]	Slag	SH + SS	Quartz powder and Quartz sand	–	–	Exposed to 200–800 °C at 5 °C/min for 1.5 h	Naturally cool down	Compressive strength, mass loss, SEM-EDS	No spalling in AAC was observed when exposed to 800 °C. The strength was retained at around 50% at 600 °C.
[116]	Slag	SH + SS	–	–	Water curing at 23 °C	Exposed to 200–800 °C at 2.7 °C/min for 1 h	Naturally cool down	Tensile strength, mass loss, SEM, MIP	The crack grew in C-A-S-H gel and the crack number and size in AAS increased with the rising temperature. At 800 °C, the pore size ranged from 0.01 to 10 μm.
[117]	Slag	SH + SS	–	–	Ambient curing	Exposed to 200–800 °C at 15 °C/min and held for 2 h	Naturally cool down	Compressive and flexural strengths, TGA, SEM, XRD	The compressive strength of slag-based AAC dropped by around 80% when exposed to 800 °C. More microcracks can be observed in ambient-cured AAC compared to heat-cured AAC.

Table 1 (*continued*)

Ref.	Precursor	Alkaline activator	Additive	Fibre	Curing method	Heating method	Cooling method	Characterisation	Main findings
[37]	Slag	Dried water glass	–	–	–	Exposed to 200–1200 °C at 5 °C/min and held for 1 h	Naturally cool down	Compressive and flexural strengths, bulk density, shrinkage, SEM, MIP, XRD FTIR, MAS NMR	Crystallisation of predominantly akermanite of slag-based AAC when exposed to above 600 °C was the main reason for the strength gain of up to 180%.
[118]	Slag	SH (2–6 M) + SS	–	–	24 h at 38 °C curing	Exposed to 300–1000 °C at 5 °C/min	Naturally cool down	Compressive strength, SEM	AAC had thermal stability when exposed to up to 500 °C.
[119]	Slag	SS	–	–	24 h at 45 °C curing	Exposed to 200–1000 °C at 6.67 °C/min (2 h)	Naturally cool down	Compressive strength, XRD, SEM-EDX	As the NaO_2 concentration in AAC increased, the reaction products became more compact and denser.
[120]	Slag	Water glass	–	–	Ambient curing	Exposed to 200–1000 °C at 10 °C/min (2 h)	Naturally cool down	Bending strength, thermal properties, MIP, SEM, XRD	The porosity of slag-based AAC increased significantly when subjected to 1200 °C.
[121]	Slag	Hydrated lime	–	–	24 h at 23 °C curing	Up to 1200 °C at 2.5 °C/min (2 h)	Naturally cool down	Compressive strength, thermal expansion, TGA	The residual strength of AAC at 200 and 800 °C are 76% and 10%, respectively.
[122]	Slag	SH (12 M)	Glass powder	–	Ambient curing	Exposed to 150–750 °C and held for 1 h	Air and water curing	Compressive and tensile strengths, mass loss, sorptivity SEM	The strength of AAS decreased with the increase of glass powder dosage. Crack initiation and propagation took place after exposed to 450 °C, along with gel structure deterioration.
[123]	Metakaolin	SH + SS	Red sand	PVA (0.5%, 1%)	Ambient curing (40 °C)	Exposed to up to 200 and 400 °C at 17 °C/min and held for 3 h	Naturally cool down	Compressive and bond strengths	A sharp drop in bond strength can be observed in the plain AAC. The addition of PVA fibres can improve the bond strength of AAC at 200 °C.
[124]	Metakaolin	SH + SS	–	–	Ambient curing	Exposed to 300 and 900 °C at 5 °C/min for 1 h	Naturally cool down	Compressive strength, crack pattern, thermal expansion, SEM, XRD, FTIR	AAMK experienced strength growth without appearance of new crystalline phases when exposed to up to 300 °C but exhibited poor volume stability, leading to thermal shrinkage.
[125]	Metakaolin	SH + SS	Basalt microfibril (5–15%)	–	Ambient curing	Exposed to 200–800 °C at 5 °C/min for 1 h	–	Compressive strength, TGA, SEM-EDS, XRD	The inclusion of basalt microfibrils can help enhance thermal resistance of AAC due to more microcracks and larger voids, and the pore-filling effect of basalt microfibrils.
[126]	Metakaolin	SH + SS	–	Micro carbon fibres	–	Exposed to 200–800 °C at 5 °C/min for 1 h	Naturally cool down	Compressive strength, volume resistivity, TGA, SEM-EDS	The addition of carbon microfibres led to more compact structure in AAC due to the pore-filling effect. The strength loss of AAC at elevated temperatures was due to thermal incompatibility.
[127]	Metakaolin	SH (5 and 10 M), SS (10 M)	Calcium hydroxide	–	Ambient curing	Exposed to 300–900 °C at 10 °C/min for 2 h	Naturally cool down	Compressive strength, MIP, XRD, FTIR, SEM-EDS	10% calcium hydroxide resulted in the formation of nepheline after AAMK was exposed to 900 °C. Sintering and densification took place. The optimum AAMK mixture contained calcium hydroxide with low activator concentration.
[128]	Metakaolin	SH (5 M) + SS	Nano-silica fume	–	–	Exposed to 500–1000 °C	–	Compressive strength, bulk density, FTIR, XRD, TGA,/DTG	The addition of nano-silica fume can improve thermal performance of AAMK with a maximum addition of 5%.

Table 1 (*continued*)

Ref.	Precursor	Alkaline activator	Additive	Fibre	Curing method	Heating method	Cooling method	Characterisation	Main findings
[23]	Fly ash and slag	SH + SS	–	–	24 h at 60 °C curing then ambient curing	Exposed to 100–800 °C at 10 °C/min for 1 h	Naturally cool down	Compressive strength, bulk density, skeleton density, open porosity, UPV, MIP, SEM-EDS, TG/DSC, FTIR, XRD	AAF exhibited better thermal stability after exposed to 600 °C, compared to AAFS with low slag content. The decomposition of hybrid N–C–A–S–H gel in AAFS led to loss of residual strength and matrix structure.
[129]	Fly ash and slag	SH + SS	Basaltic pumice aggregate	–	48 h at 80 °C oven curing, then ambient curing	Exposed to 100–800 °C at 6 °C/min for 3 h	Naturally cool down	Compressive strength, water absorption, SEM-EDS, XRD, PLM	The increase of slag content in AAFS resulted in a decrease in compressive strength of AAFS after exposed to elevated temperatures.
[33]	Fly ash and slag	SH (10 M) + SS	–	–	24 h at 70 °C oven curing, then ambient curing	Exposed to up to 300–700 °C at 10 °C/min and held for 2.5 h	Naturally cool down	Compressive strength, mass loss, volume change, TGA/DTG, SEM-EDS-XRD	AAC containing 100% fly ash had the best mechanical performance at 500 °C and 700 °C, while fly ash-slag based AAC had low strength loss at 500 °C and 700 °C.
[130]	Fly ash and slag	SH (12–20 M) + SS	–	–	24 h at 60, 70 °C oven curing	Exposed to 200 °C for 1 h	–	Compressive and flexural strengths	The compressive strength of AAC with 20 M was less than that of AAC with 16 M, which increased with the increase of sodium silicate.
[131]	Fly ash and slag	SH + SS	–	–	48 h at 80 °C oven curing then ambient curing	Exposed to 200–800 °C	–	Compressive and flexural strengths, physical properties, SEM, EDS, PLM, XRD	The inclusion of fly ash in slag-based AAC can increase the thermal resistance and reduce the mass loss. Na content in AAC increased at elevated temperatures.
[132]	Fly ash and slag	SH (8–14 M) + SS	–	–	24 h at 60–100 °C heat curing and ambient curing	Exposed to 200–2000 °C at 4 °C/min	Naturally cool down	Compressive strength, mass loss, setting time, SEM-EDS	The addition of slag in fly ash-based AAC led to effective polymerisation and strength gain. When AAC exposed to 600 °C, there was a change from crystalline phase to amorphous phase.
[133]	Fly ash and slag	SH + SS	–	–	–	Exposed to 400–1000 °C at a rate of ISO834	Naturally cool down	Compressive strength and splitting tensile strengths	Compared to PCC, AAC had more obvious surface change after exposed to 400–600 °C.
[134]	Fly ash and slag	SH + SS	Waste ceramic powder	–	Ambient curing	Exposed to 400–900 °C	Air cooling	Compressive strength, mass loss, UPV, TGA, XRD, SEM-EDX, FTIR	The addition of waste ceramic powder at dosages of 50–70% can improve thermal resistance of slag-based AAC at up to 900 °C. However, when adding fly ash into the mixture, the strength dropped.
[26]	Fly ash and slag	SH + SS	–	–	Ambient curing	Exposed to 300 and 600 °C at 4 °C/min for 1.5 h	–	Compressive strength, XRD, FTIR, SEM	The change in slag content in fly ash-slag based AAC resulted in various mechanical responses when exposed to elevated temperatures. The recommended mixture consisted of 90% fly ash and 10% slag.
[135]	Fly ash and slag	SH + SS	–	–	48 h at 40 °C curing, then ambient curing	Exposed to 300–1100 °C at 2 °C/min	–	Compressive strength, DTG, XRD, SEM	Fly ash and slag-based AAC exhibited the lowest compressive strength when exposed to 700 °C. At 700 °C, the porosity reduced while a new crystalline phase was found along with sintering at 1000 °C.
[136]	Fly ash and slag	SH + SS	–	–	–	Exposed to 400 °C for 1 h; 600 °C for 1 h, 600 °C for 2 h	Naturally cool down	Compressive, tensile and flexural strengths	The cracks in AAC induced by elevated temperatures were more intense and wider than those in PCC.

Table 1 (*continued*)

Ref.	Precursor	Alkaline activator	Additive	Fibre	Curing method	Heating method	Cooling method	Characterisation	Main findings
[137]	Fly ash and slag	SH (14 M) + SS	–	–	60 °C oven curing for 5–168 h	Exposed to 200–800 °C at 5 °C/min	Naturally cool down	Compressive and flexural strengths, bulk density, apparent porosity, water absorption	The recommended curing condition was 48 h at 60 °C for the mixture made from 14 M SH. 400 and 600 °C were identified as the critical temperature points, at which the compressive strength of AAC dropped and physical changes occurred.
[138]	Fly ash and slag	SH + SS	Silica fume	–	Ambient curing	Exposed to 200–800 °C at 10 °C/min and held for 2 h	Natural and water cooling	Compressive strength, mass loss, UPV, FTIR, SEM	AAC after water cooling had a more significant degradation at elevated temperatures compared to the ones with natural air cooling.
[139]	Fly ash and slag	SH (8 M) + SS	–	–	22 h at 80 °C curing then ambient curing	Exposed to up to 800 °C at 2.5 °C/min and held for 1 h	Naturally cool down	Compressive strength, Stress-strain	The increased compressive strength of AAC after exposed to 800 °C was ascribed to the further hydration of unreacted particles and sintering reaction.
[140]	Fly ash and slag	SH (3.5–10 M) + SS	Zirconia, Alumina, Zinc oxide, Silica fume	–	Ambient curing	Exposed to 200–800 °C at 10 °C/min and held for 2 h	Naturally cool down	Compressive and tensile strengths, water absorption, TGA, SEM	AAF had more resistance to temperature compared to AAFS. The presence of more compact and homogeneous gels appeared after exposure to 800 °C.
[141]	Fly ash and slag	SH (4 M)	Soda lime waste glass		Ambient curing	Exposed to 200–800 °C at 5 °C/min and held for 2 h	Naturally cool down	Compressive strength, mass loss, thermal expansion, SEM	The reduced compressive strength of AAFS after high temperature exposure was owing to the increase of slag content. The melting of waste glass at 600–800 °C led to the increase of thermal resistance.
[142]	Fly ash and slag	SH (10 M) + SS	–	PVA fibres	Ambient curing	Exposed to 105–800 °C at 10 °C/min and held for 2 h	Naturally cool down	Compressive and tensile strengths, mass loss, UPV, DSC, TGA, XRD, MIP, SEM	Mechanical properties of PVA fibre reinforced AAFS was affected by phase composition, microstructure evolution and fibre bridging effect. The sintering effect occurred after 600 °C in AAFS, leading to the reduction of small gel pores and increase of larger pores due to formation of cracks.
[143]	Fly ash and metakaolin	KOH + K₂SiO₃	Silica fume	–	–	Exposed to 100–700 °C at 5, 8 and 12 °C/min	–	Compressive strength, spalling, Sorptivity, XRD	AAC had better spalling-resistance and higher water absorptivity than PCC. The sintering reaction occurred at 700 °C.
[144]	Fly ash and metakaolin	KOH + K₂SiO₃	–	–	Ambient curing	Exposed to 100, 300, 500 and 700 °C at 5 °C/min	–	Compressive, splitting tensile and bond strengths	The bond strength of AAC reduced when exposed to 300 °C. The bond strength and tensile strengths of AAC dropped at a greater pace compared to its compressive strength.
[145]	Fly ash and metakaolin	KOH + K₂SiO₃	–	–	Ambient curing	Exposed to 100–700 °C	–	Compressive, tensile, bond and bending strengths, thermal expansion TGA/DTG, DSC	The flexural, compressive, tensile and bond strengths of AAC increased up to 100 °C, followed by a decrease when exposed to 300–700 °C. The mass loss was induced by thermal incompatibility and dehydration.
[36]	Fly ash and metakaolin	KOH + K₂SiO₃	–	–	–	Exposed to up to 800 °C at 10 °C/min and held for 2 h	Naturally cool down	Compressive and bending strengths, thermal expansion TGA/DTG, SEM-EDS, MIP	Compared to fly ash-based AAC, AAMK concrete had a more compact and denser microstructure due to greater thermal shrinkage and less pore evolution.

(continued on next page)

Table 1 (*continued*)

Ref.	Precursor	Alkaline activator	Additive	Fibre	Curing method	Heating method	Cooling method	Characterisation	Main findings
[146]	Fly ash and metakaolin	SH + SS	–	–	24 h at 40 °C curing then curing at 40 °C	Exposed to 100–800 °C at 2 °C/min and held for 2 h	Naturally cool down	Compressive strength, mass loss, thermal shrinkage, MIP, SEM	A strength gain of fly ash and metakaolin-based AAC happened when exposed to up to 500 °C, whose microstructure became denser after 400 °C.
[35]	Fly ash and metakaolin	SH (10 M) + SS	–	–	24 h at 40 °C curing then curing at 40 °C	Exposed to up to 1000 °C at 2 °C/min	Naturally cool down	Compressive strength, mass loss, thermal shrinkage, SEM	A denser and more compact microstructure of metakaolin and fly ash-based AAC was detected after exposed to 400 °C due to sintering effect and geopolymerisation.
[147]	Slag and metakaolin	SH and SS	Clag brick waste powder	–	24 h at 105 °C heat curing then water curing	Exposed to up to 800 °C	–	Compressive strength, SEM	With the increase of temperature from 100 to 400 °C, the compressive strength went up.
[148]	Slag and metakaolin	–	PVA resin powder	–	–	Exposed to 150–850 °C at 3 °C/min and held for 1 h	Naturally cool down	Compressive and flexural strengths, mass loss, volume shrinkage, XRD, SEM	The compressive strength increased at 150–300 °C, followed by a decrease at 450–800 °C due to dehydration of AAC matrix.
[149]	Slag and tailing	SH + SS	–	–	Ambient curing	Exposed to 200–1200 °C at 10 °C/min and held for 2 h	Cool down by electric fan	Compressive strength, thermal expansion, TGA, DSC, XRD, FTIR	AAC experienced cracking and shrinkage due to dehydroxylation at 300–700 °C and thermal expansion of AAC can be observed after 800 °C.
[150]	Slag and palm oil fuel ash	SH (12 M) + SS	–	–	–	Exposed to 100–800 °C at 5 °C/min	Naturally cool down	Compressive strength, TGA, DSC, XRD, FTIR	The substitution of slag by palm oil fuel ash indicated the role of aluminium in the development of C-(A)-S-H gel.
[151]	Fly ash and palm oil fuel ash	SH + SS	–	–	24 h at 65 °C curing then ambient curing	Exposed to 200–1000 °C at 5 °C/min and held for 2 h	Naturally cool down	Compressive strength, TGA, XRD, SEM	All the mixtures can gain strength when exposed to up to 500 °C. The pore size increased significantly with the increase of temperature to 800 °C.

Note: SH – sodium hydroxide; SS – sodium silicate; PVA – polyvinyl alcohol.

stress induced damage is the dominant factor, while pore pressure induced damage is the main contributor to concrete failure if the slow heating rate is employed [160].

After exposure to 100 °C, physically bound water evaporates and chemically bound water can be released from the C–S–H layer, along with the decomposition of C–S–H gel that leads to an unstable structure. At 400–600 °C, calcium hydroxide (CH) in PCC can decompose into calcium oxide and water. After 700 °C, the decarbonation of calcium carbonate ($CaCO_3$) takes place. When the temperature reaches 800 °C, all chemically bound water can be fully evaporated [152].
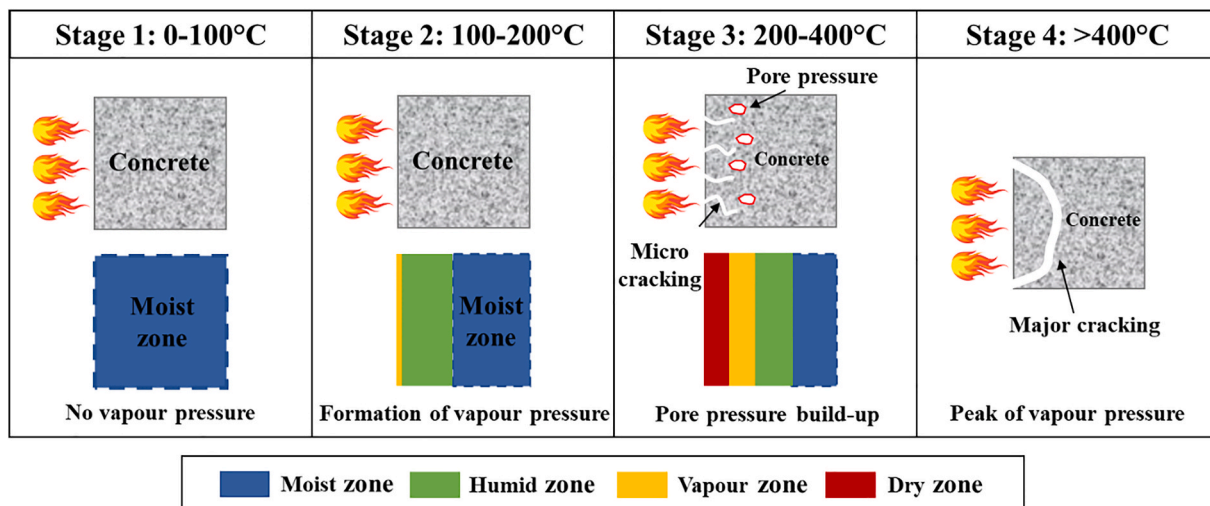

Fig. 3. Schematic illustration of damage evolution in Portland cement concrete (PCC) at elevated temperatures [162].
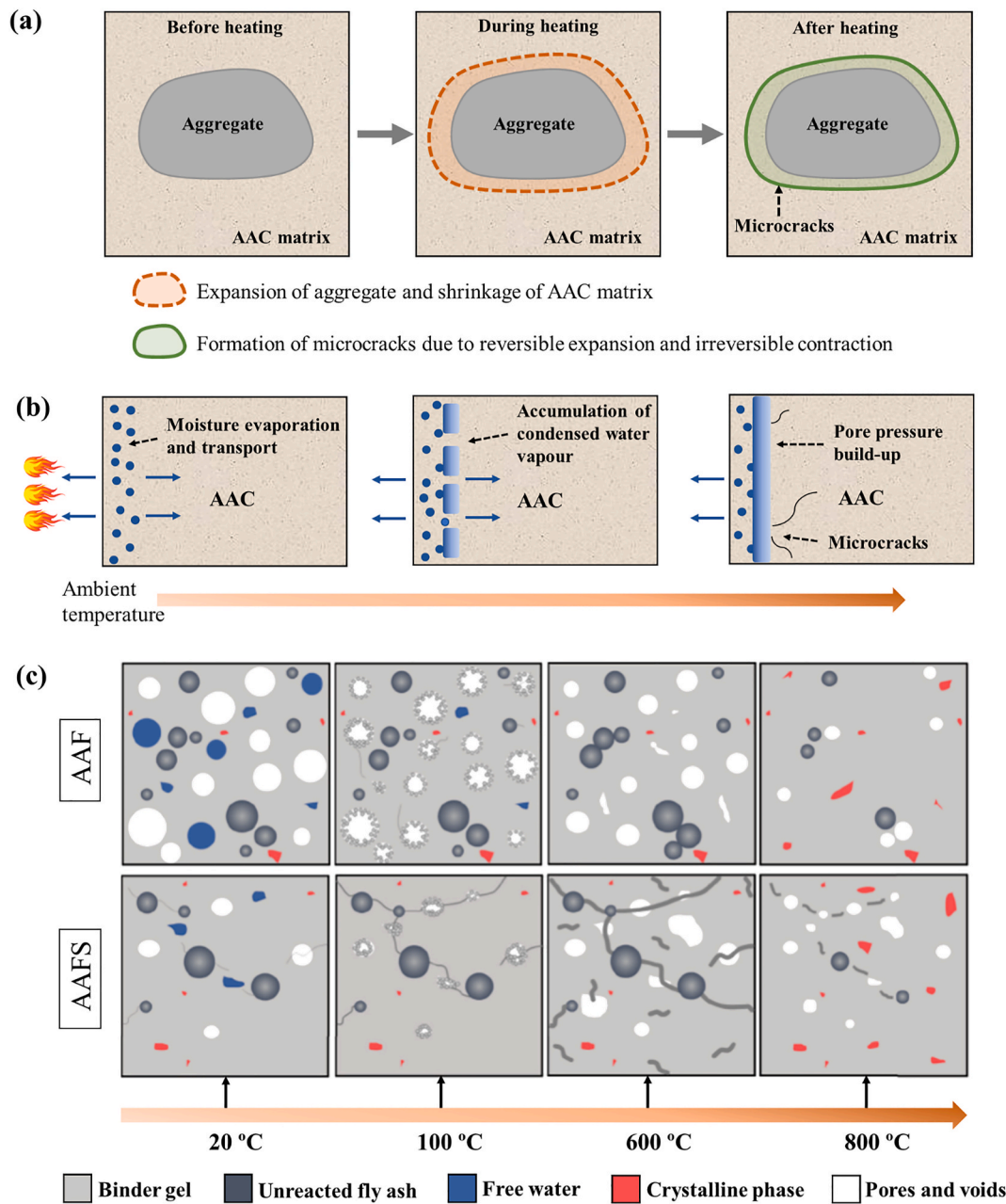
Fig. 4. Damage mechanisms of AAC at elevated temperatures: (a) thermal incompatibility, (b) pore pressure build-up, and (c) phase transformation (adapted from Refs. [23,27,162,167]).

3.2. Alkali-activated concrete

In comparison with the PCC system, AAC exhibits better high-temperature resistance [11,163,164]. This is because that alkali-activated aluminosilicate gels in AAC differ from cement paste in PCC [28,163]. A sodium or potassium-based alkaline activator is needed to react with silica- and alumina-rich phases, due to the non-hydrated aluminosilicate gel binding phases in AAC matrix, leading to the generation of gels without much chemically bounded or physically absorbed water compared to C–S–H gels in PCC [11]. Thus, an open pore structure of AAC matrix is formed, which can result in a higher resistance to withstand elevated temperatures of up to 600–1200 °C with less strength loss compared to PCC [25,107].

The damage mechanisms in AAC at elevated temperature were found to be similar to PCC system, which include: (1) thermal incompatibility, (2) pore pressure build-up, and (3) phase transformation [24], as illustrated in Fig. 4. The first mechanism occurs when heat flow transfers in AAC. As different phases in AAC (i.e., matrix and aggregates) have different thermal conductivity and thermal capacity, there exist non-uniform distribution of heat flow and inhomogeneity of thermal stress inside AAC, leading to the initiation of cracks and strength degradation [24]. At the initial state, there is no expansion or shrinkage in AAC. When exposed to elevated temperatures, the expansion of aggregates and contraction of AAC matrix take place. The microcracks are then formed inside AAC due to the reversible expansion and irreversible shrinkage after heating, which have a detrimental impact on residual strength of AAC [27]. However, it was found that the mechanical performance of AAF at elevated temperatures was unstable. As the temperature rises, viscous sintering takes place, which denotes the collapse of nano-pores and development of interparticle bonding, resulting in the self-healing of micro-cracks and densification of concrete matrix [165]. Moreover, further chemical reaction can enhance the strength of AAF,

whereas the thermal incompatibility induced damage has a reverse effect [24].

The pore pressure effect is associated with the transportation of water/moisture and accumulation of pore pressure as mentioned above for PCC, which is considered as one of the main contributors to the deterioration of AAC during exposure to high temperatures. The trapped moisture and vapour can result in cracking and damage to the pore structure. For different alkali-activated systems, AAF concrete performs better than AAMK at elevated temperatures, due to more small pores in AAF concrete with an inter-connected network that can hinder the vapour pressure build-up in pores [28].

The phase transformation is related to the effects of different raw materials, alkali cations and calcium content and can form a combined effect together with pore pressure build-up on AAC at elevated temperatures [18,24,166]. Fig. 4c displays a comparison of the damage evolution in single and blend precursor systems (i.e., AAF and AAFS) at elevated temperatures. At ambient temperature, AAF has a porous structure with some unreacted fly ash particles and free water. At 100 °C, the pore pressure induced by water evaporation can be released through the porous network in AAF without formation of major cracks. Meanwhile, further geopolymerisation takes place, leading to strength gain as the newly formed gels can fill the cracks and voids left by free water. After exposure to 100–600 °C, AAF remains stable with no significant loss of structure integrity and change of crystalline phases. The shrinkage of AAF matrix and viscous sintering can be detected at 600 °C and new crystalline phases are formed after 800 °C. The re-crystallisation process can weaken the gel skeleton with a less compact texture, while the sintering reaction can continue to compact and strengthen the AAF matrix by filling the pores and cracks [23]. Thus, there is a combined effect of both strength gain and loss on AAF, which may retain the residual strength of AAF when exposed to 800 °C.

Regarding the blend precursor systems, AAFS exhibits a relatively more compact structure with less unreacted particles and residual water before high temperature exposure, which can be ascribed to the incorporation of slag that accelerates the reaction process, resulting in a denser matrix compared to AAF [23]. Some microcracks can be observed in AAFS matrix at this stage. When exposed to 100 °C, the initiation of new cracks and propagation of existing cracks can happen in AAFS due to the pore pressure trapped in a compact structure with poor internal connectivity. Meanwhile, AAFS experiences further geopolymerisation that can strengthen the internal structure by filling the pores and voids. At 600 °C, gel decomposition occurs in AAFS, resulting from slag that forms hybrid N–C-A-S-H gel with lower thermal stability compared to N-A-S-H gel in AAF [23]. The decomposition of hybrid gels can lead to the initiation of small cracks, and thus significantly deteriorate the strength of AAFS at this stage. Similar to AAF, the formation of new crystalline phases and viscous sintering are the dominant factors that affect the residual strength of AAFS at 800 °C. Nevertheless, AAFS suffers more from the decomposition of matrix leaving larger cracks and voids compared to AAF, and thus a greater strength loss. In general, the addition of slag plays a key role in the damage mechanism of AAFS, which has a more complex and unstable gel structure compared to the single precursor system, i.e., AAF.

4. Microstructural characteristics of AAC at elevated temperatures

Microscopic properties reflect the fundamental changes in AAC at elevated temperatures such as phase transformation and microstructural and pore structure evolution, which can explain the damage mechanisms and essentially affect the macroscopic performance of AAC at elevated temperatures. Table 2 summarises the experimental studies on microstructural characteristics of AAC at elevated temperatures, including single and blend precursor systems (AAF, AAS, AAMK and AAFS).

4.1. Phase stability

4.1.1. Single precursor system

Phase transformation can affect the behaviour of AAC in single precursor systems subjected to elevated temperatures. The matrix structural evolution can be evaluated through XRD analysis [31]. Fig. 5 gives a summary of the main phase changes observed in different types of AAC. In AAF, the geopolymerisation can primarily result in the formation of amorphous aluminosilicate gel (three-dimensional N-A-S-H type gel) to promote strength and durability at ambient temperature [11,168,169]. The main semi-crystalline phases include quartz (SiO_2),

Table 2
Summary of phase changes of AAC at elevated temperatures.

Ref.	Precursor	Main findings
[31]	Fly ash	Appearance of crystalline phases (albite, anorthite, and magnetite) after 800 °C
[32]	Fly ash	Increase in the amorphous phase content after 800 °C
[103]	Fly ash	Appearance of albite and nepheline at 300 °C, and more albite was observed at 900 °C
[34]	Fly ash	Hydroxysodalite and herschelite disappeared to form albite and nepheline after 600 °C
[176]	Fly ash	Disappearance of hydroxysodalite and formation of nepheline at 800 °C
[96]	Fly ash	Peaks of quartz, mullite and hematite and appearance of albite and nepheline at 1000 °C
[114]	Slag	Formation of new crystalline phases of gehlenite, larnite and mayenite at 1000 °C
[37]	Slag	Crystallisation to form akermanite, diopside and wollastonite at 1200 °C
[177]	Slag	Increase of akermanite and formation of gehlenite and merwinite at 800 °C
[117]	Slag	Increase of albite and sodium-aluminium-silicate after exposed to 800 °C
[124]	Metakaolin	Formation of new crystalline phase of nepheline at 900 °C
[178]	Metakaolin	Formation of nepheline after firing to 1000 °C
[33]	Fly ash and slag	No formation of new crystalline phase after exposed to 700 °C
[26]	Fly ash and slag	No new crystalline phases detected and decomposition of calcite at 600 °C (50% slag)
[179]	Fly ash and slag	Formation of akermanite, gehlenite, anorthite and nepheline at 800 °C (25, 50, 75% slag)
[38]	Fly ash and slag	New crystalline phases: anorthite, nepheline and wollastonite at 600 °C
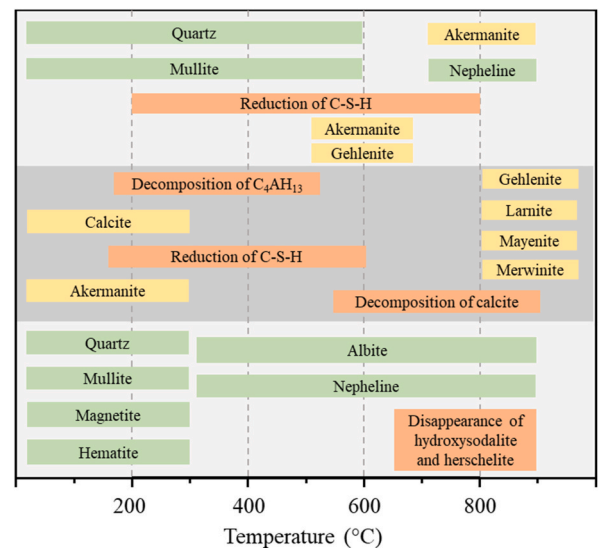
Fig. 5. Schematic diagram of phase changes in different types of AAC at elevated temperatures.

mullite ($Al_6Si_2O_{13}$), magnetite ($Fe + 2Fe_2 + 3O_2$) and hematite (Fe_2O_3) [31,101,103]. Quartz is a common phase in unreacted fly ash particles with a high melting point of 1713 °C, which can be primarily in origin and formed from the Al_2O_3–SiO_2 system [170]. Mullite is a refractory with a melting point of 1830 °C [171] that is stable at both room and elevated temperatures and contributes to thermal resistance, mechanical properties and thermal stability with low thermal conductivity and expansion [96,172–174]. As summarised in Table 2, before 300 °C, the reduction of Si–O–Al and Si–O–Si can be observed, implying the absorption of weak bond molecules at this stage [32]. The phase changes mainly happen with the appearance of new crystalline phases including albite ($NaAlSi_3O_8$) and nepheline ($NaAlSiO_4$) after exposure to 300–1000 °C, whereas other phases are relatively stable at 1000 °C. The formation of albite and nepheline is associated with the disappearance of minority zeolite crystalline phases including hydroxysodalite ($Na_4Al_3Si_3O_{12}OH$) and herschelite ($NaAlSi_2O_6 \cdot 3H_2O$) after exposure to 600 °C [34]. Also, the appearance of nepheline phases can contribute to the mass loss of AAF matrix at 750 °C [39,175].

It is noteworthy that alkaline activators can affect the phase stability of AAF at elevated temperatures. Potassium-based (KOH and K_2SiO_3) and sodium-based (NaOH and Na_2SiO_3) activators are the most commonly used ones to produce AAC. At 400 °C, more mullite can be detected in AAF with 2% nano silica activated by potassium activators compared to sodium activators, which is a high temperature phase that can contribute to the strength gain of AAF exposed to elevated temperatures [91]. A slightly higher content of amorphous phase can be observed in AAF made from potassium activators compared to the sodium counterparts, which can enhance the mechanical strength of AAF at elevated temperatures. Furthermore, the molarity of alkaline solutions can also influence the crystalline phases of AAF. The increase of molarity of NaOH solutions can improve the residual strength of AAF at high temperatures, which can be ascribed to the high amount of sodium oxide contained in the solutions, enhancing the aluminosilicate phase to promote further geopolymerisation. The formation of Na-based crystalline phases such as albite and nepheline that have great thermal stability with high melting points can improve the thermal resistance and thus mitigate the strength loss of AAF at elevated temperatures [98,180].

In AAS, the unreacted slag has high calcium concentration that contains crystalline phases such as calcite ($CaCO_3$) and akermanite ($Ca_2Mg(Si_2O_7)$) [33,114]. After mixing with alkaline activators (i.e., NaOH and Na_2SiO_3), the strength of AAS is developed with the formation of a C-(A)-S-H type gel. Compared to AAF, there are additional hydrated phases in AAS due to the high calcium content, which can impair the thermal resistance and stability [11]. No obvious new phases appear in AAS until the temperature goes up to 300 °C, where the decomposition of C_4AH_{13} occurs along with the drop in C–S–H gel content, indicating the structural evolution of C–S–H layers [26]. After exposed to 600 °C, the calcium hydrates decompose with de-carbonation of calcite at around 756 °C [26,114]. With the rise of exposure temperature to 800–1000 °C, the new crystalline phases such as gehlenite ($Ca_2Al_2SiO_7$), larnite (Ca_2SiO_4), mayenite ($Ca_{12}Al_{14}O_{33}$) and merwinite ($Ca_3Mg(SiO_4)_2$) can be observed. The crystallisation of amorphous phases leads to a more ordered structure with these stable crystalline phases, which can enhance the mechanical properties of AAS matrix due to sintering effect and densification at high temperatures [5,114,181, 182]. Minor crystalline phases such as diopside ($CaMgSi_2O_6$) and wollastonite ($CaSiO_3$) disappear when the temperature goes up to 1150 °C [37].

For AAS made from waterglass solution, there is an increase of the amount of akermanite in matrix when exposed to 800 °C compared to lower temperatures. When continuing heating until 1200 °C, the development of akermanite is further promoted due to high temperature environment [120]. However, the formation of this crystalline phase is not directly associated with the mechanical properties of AAS at elevated temperatures.

Regarding AAMK, amorphous aluminosilicate gel exists with the crystalline phases such as quartz and anatase (TiO_2) [11]. High-temperature exposure up to 300 °C has a limited effect on the phase changes or transformation. The new crystalline phase of nepheline can be detected as the temperature goes up to 900 °C due to geopolymerisation along with reordering of amorphous aluminosilicates [124,178,183]. In general, AAF exhibits better thermal stability and less damage than AAMK after high temperature exposure as AAMK contains more free moisture and thus can lead to a more pronounced pore pressure within the matrix [11,184].

4.1.2. Blend precursor system

As a combination of AAF and AAS, the reaction products in AAFS are more complex, mainly consisting of N-A-S-H (from AAF), C-A-S-H (from AAS) and N–C-A-S-H (a hybrid of AAF and AAS) gels [33,131]. In AAFS matrix, the fly ash/slag ratio is the dominant factor that affects the formation of different phases [26]. The XRD patterns of AAFS before and after exposure to up to 400 °C exhibit insignificant differences, except a slight reduction of C–S–H phase that indicates the dehydration. There is almost no difference between the crystalline phases of AAF and AAFS (with no more than 20% slag) at 600 °C, which mainly contains quartz and mullite [26], while akermanite and gehlenite can be detected in AAFS containing no less than 50% slag [38]. At 700 °C, AAFS with 40% slag content can contain C–S–H with traces of calcite as seen in the XRD patterns [33]. Moreover, the intensity of C–S–H in AAFS reduces significantly at elevated temperatures, while there is no obvious impact on that in AAS, implying that the incorporation of fly ash and slag can change the nature and the main binding phases [26].

At 800 °C, crystalline phases such as akermanite, gehlenite, anorthite ($CaAl_2Si_2O_8$) and a small amount of nepheline can be observed in AAFS [179], along with the disappearance of C–S–H phase, indicating fully crystallisation or dehydration in all AAFS mixtures containing slag dosages of 25%, 50% and 75%, which is consistent with that reported in Ref. [38]. As the C–S–H gel is susceptible to high temperature damage, AAFS with higher slag content is prone to suffering more serious strength retrogression due to the higher calcium concentration that results in the formation of additional hydrates compared to AAF [11,179]. In addition, the amounts of gehlenite and anorthite are strongly related to the Ca/Al ratio in AAFS as higher slag content can lead to the dominant formation of gehlenite, while the opposite situation can lead to the dominant formation of anorthite [179].

Regarding other blend types of AAC such as alkali-activated fly ash-metakaolin and alkali-activated slag-metakaolin systems (see Table 1), a new crystalline phase can be detected in alkali-activated fly ash-metakaolin specimens when exposed to 500–700 °C, resulting from the sintering reaction of unreacted fly ash particles [143] and the slag content and alkalinity can affect the existence of C–S–H phase in alkali-activated slag-metakaolin system [148]. However, the phase stability of AAC in blend precursor system at elevated temperatures has not been systematically explored with respect to different factors such as types of alkaline activators, curing condition and so on. Thus, further research is required to gain an in-depth understanding of the phase changes and the effects of different factors on the phase stability of AAFS at elevated temperatures.

4.2. Microstructural evolution

4.2.1. Single precursor system

Microstructure of AAC at elevated temperatures can be affected by various factors in relation to different damage mechanisms. The changes in porosity, pore size and pore connectivity of AAC with exposure temperatures are directly related to moisture transport inside the matrix and pore pressure-induced damage [3]. Fig. 6 demonstrates an example of AAF exposed to elevated temperatures. At ambient temperature, AAF matrix exhibits a porous structure with unreacted spherical/semi-spherical fly ash particles, N-A-S-H gel as a dense and
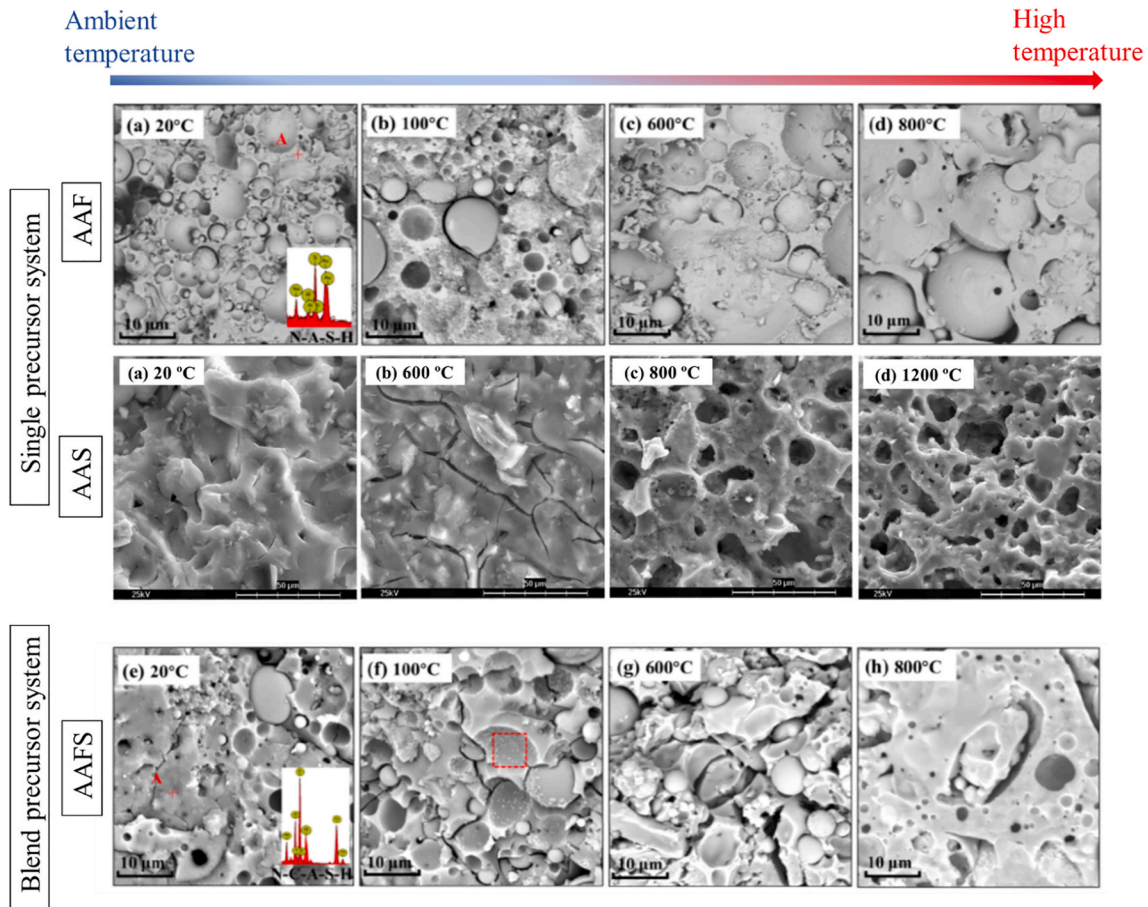
Fig. 6. SEM micrographs of AAF, AAS and AAFS samples exposed to different temperature levels, (adapted from Refs. [23,37]).

bulky base and some stripe-shaped substances by abundancy of alkaline [31,33], which is corresponding to the semi-crystalline phases such as quartz and mullite mentioned in the previous section. After exposed to 200 °C, many unreacted fly ash particles can be observed [32]. The microstructural evolution of AAF is mainly associated with the evaporation of free moisture, which can cause the accumulation of entrapped vapour pressure and initiation of microcracks [18].

From 200 °C to 400 °C, further evaporation of bounded moisture between alkali-activated binder and unreacted fly ash particles occurs with the development of microcracks [31]. As the temperature goes up from 400 °C to 600 °C, more porous internal structures can be detected with either few or nonreacted fly ash particles remaining [31,32]. Also, sintering reaction and densification take place at about 550 °C and above [3]. At 800 °C, further augment of voids and thermal stress induced microcracks could lead to a significant loss of strength of AAF matrix [27,31,32]. AAF with class F fly ash has a looser and more honey-comb shaped structure, while AAF with class C fly ash exhibits a denser matrix [31]. This indicates the influence of precursor type and mix proportion on the microstructural features of AAF at elevated temperatures. Above 800 °C, the melting of matrix with a smoother texture and less impurities can be detected in AAF due to viscous sintering that heals the microcracks at high temperatures [11,33,147,185]. Fig. 7 illustrates the pore size distribution of AAF at elevated temperatures. The main peak shifts from a smaller pore size (<0.1 μm) to a larger one (>1 μm) after exposure to 800 °C, indicating the sintering and densification effect on the pore structure changes of AAF. New crystalline phases such as albite and nepheline can also be observed with the disappearance of hydroxysodalite and herschelite at this temperature level, and there is an increase in pore size and volume compared to the unexposed AAF at 800 and 1000 °C.

In AAS concrete, the matrix shows a smooth surface with some unreacted slag particles and microcracks at ambient temperature [114, 186]. C-A-S-H gel is structurally stable due to the adhesive forces from those saturated small pores [37]. As temperature rises, the moisture is gradually released from the small pores and migrates inside AAS matrix. The evaporation of free moisture and slight decomposition of C-A-S-H gel lead to the development of microcracks and deterioration of AAS matrix at up to 200 °C [37]. From 200 °C to 600 °C, the initiation and propagation of microcracks take place due to the dehydration of binder and reduction of C–S–H gel [37,114,177]. Consequently, the strength could be further degraded due to the loss of water [37]. Partially reacted slag particles appear in various sizes with irregular shapes and the amount of unreacted slag particles decreases accordingly. Upon exposure to 600 °C, the pore size and volume increase with the appearance of larger cracks [37,114,177]. The stability of C-A-S-H structure suffers from high temperature exposure and the dehydroxylation and crystallisation happen, leading to the damage in AAS matrix as the temperature rises from 600 °C to 800 °C [114]. The phase transformation (e.g., formation of akermanite) at 800 °C correspondingly results in the evolution of microstructure and mechanical properties, as akermanite has a week and porous structure that leads to densification, increase of pore sizes and strength loss of AAS at this temperature level [37,117,177,187, 188]. From 800 °C to 1000 °C, the shrinkage of gel and densification occur in AAS matrix due to melting and sintering, leading to the formation of a smooth and compact structure [114]. Less microcracks along with the reduction of gel pores in a connected network can be observed at this stage, implying the strength recovery of AAS matrix after exposed to 1000 °C [114,184,189].
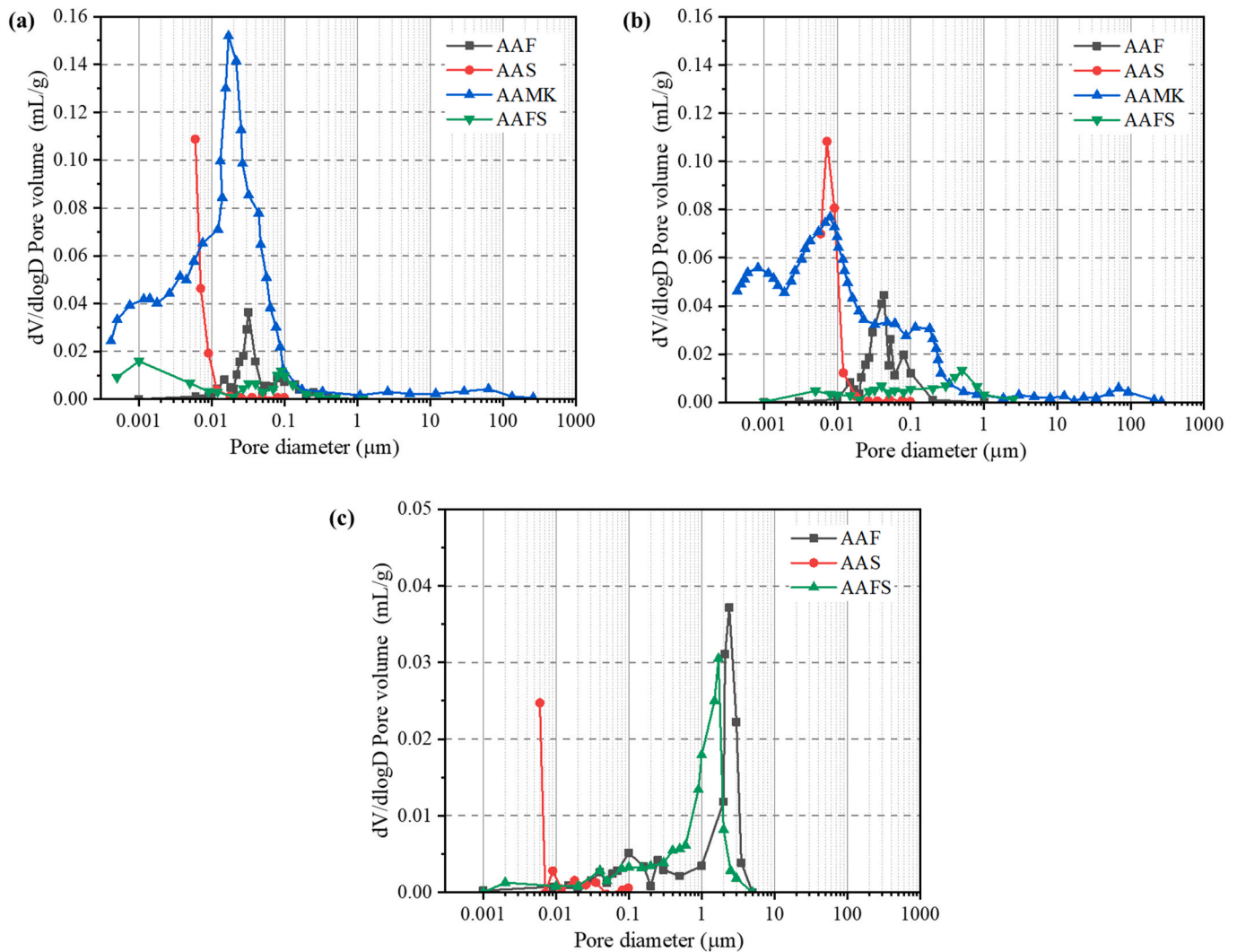
Fig. 7. Pore size distribution of AAC at (a) ambient temperature and exposed to (b) 400 °C and (c) 800 °C (adapted from Refs. [23,37,146]).

4.2.2. Blend precursor system

At ambient temperature, unreacted fly ash and slag particles can be found within AAFS matrix. The unreacted fly ash particles exhibit the aforementioned quartz and mullite, whereas calcite can be identified in the unreacted slag particles [26,190–193]. When the temperature increases to 200 °C, the porosity of AAFS matrix drops (reduction of fraction of pores with diameter of 5–10 nm) along with the strength rise, which can be ascribed to the formation of an additional highly cross-linked gel product, making the matrix denser [38,179]. At 300 °C, the microstructure of the gel is stable without obvious changes. For AAFS containing 40–50% slag, there exist C-A-S-H type gel and/or N-(C)-A-S-H gel with a slight decomposition of C-A-S-H gel [26,33]. For AAFS matrix with low slag content (≤20%), the primary binding phase of low calcium N-(C)-A-S-H type gel is structurally stable at 300 °C [33], while the remnant fly ash particles continue to react (i.e., a shift of T-O bond towards a higher rate of recurrences indicating the strengthened Si content in N-A-S-H gel [26,194]), which promotes the formation of N-A-S-H or N-(C)-A-S-H gel, leading to a more homogeneous structure with strength gain at 300 °C [33].

From 200 °C to 400 °C, the porosity of AAFS (pore diameter of 0.005–6 μm) is further reduced and the reaction of the residual fly ash particles continues at elevated temperatures, leading to the rise in strength [38]. On the other hand, the strength of AAFS is found to decrease at 300–500 °C, due to the moisture evaporation and the replacement of Ca by Na that degrades the thermal stability of zeolite

materials at elevated temperatures [33,37]. Moreover, as the slag content in AAFS drops from 40% to 20%, the strength loss reduces, while AAFS with higher slag content is less stable at elevated temperatures as the slag has a high CaO content with relatively lower glass transition point [33]. After exposed to 600 °C, further dehydration of C-A-S-H phase takes place with the presence of crystalline phases of akermanite and gehlenite, while the formation of anorthite is associated with N-(C)-A-S-H gel [38]. At 600 °C, calcite disappears in AAFS with 50% slag and N-(C)-A-S-H is recognised as the dominant binder gel in AAFS with 10% slag [26].

At 800 °C, the pore size of AAFS matrix increases (pore diameter >6 μm) with the disappearance of C–S–H phase [38]. The C-A-S-H gel produced from slag is fully dehydrated along with the crystallisation of akermanite and gehlenite, while the N-A-S-H gel generated from fly ash is partially crystallised with the formation of nepheline and the N-(C)-A-S-H gel come from both fly ash and slag is crystallised to form anorthite [38]. The porosity of AAFS matrix declines with the increase of slag content from 25% to 75% [179], as the fly ash-related products of anorthite and nepheline have porous structure. Therefore, the fly ash/slag ratio can greatly affect the crystalline phases and microstructure of AAFS. In general, the increase of slag content in AAFS can result in a higher strength loss due to thermal instability of CaO, but it can also lead to a denser and more compact microstructure, reducing the deterioration of AAFS at elevated temperatures [33]. In comparison with AAF, AAFS exhibits a higher proportion of gel pores (<0.01 μm),
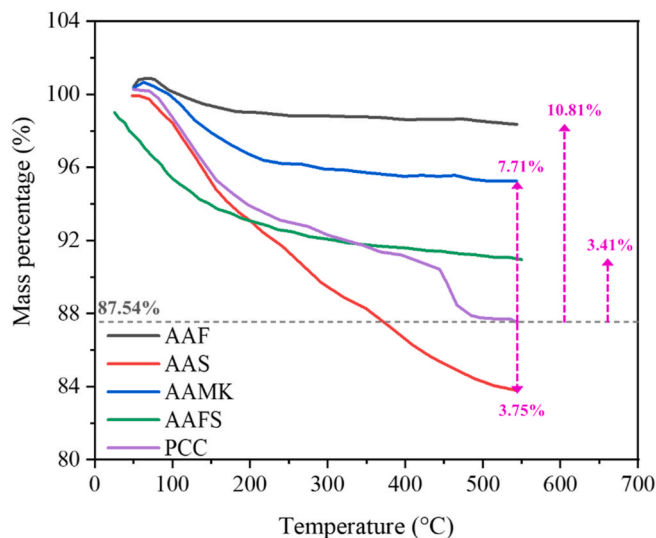
Fig. 8. Mass loss of AAC and PCC at elevated temperatures (adapted from Refs. [11,23]).

Fig. 9. Thermal deformation of AAC and Portland cement concrete (PCC) at elevated temperatures, along with a schematic illustration for AAF (adapted from Refs. [19,39,121,124,141]).

indicating that a higher degree of reaction takes place in AAFS matrix at ambient temperature, as seen in Fig. 6a [23]. Similar pore size distribution of AAFS and AAF can be observed at 800 °C, where the main fraction of pores is at around 2 µm, owing to further geopolymerisation, contraction of gel matrix and sintering effect.

5. Thermal properties of AAC at elevated temperatures

5.1. Thermal stability

Thermal stability of AAC plays a crucial role in its behaviour at elevated temperatures, which can be estimated through thermogravimetric analysis (TGA). Fig. 8 presents the mass loss of PCC and different types of alkali-activated pastes at elevated temperatures [11], indicating that AAF paste exhibits the lowest mass loss of less than 2% in comparison with AAMK, AAS and PCC pastes. The majority of mass loss of AAF paste occurs at 100–200 °C, which can be ascribed to free water evaporation [11,28,104]. After the initial decline, the mass of AAF paste gradually tends to be stable at 250–800 °C [28]. The slight mass loss at this stage can be attributed to the liberation of water during further geopolymerisation and the formation of new crystalline phases such as albite and nepheline [11]. Compared to AAF, AAMK paste performs slightly worse with a mass loss of approximately 4.75%. The relatively higher water/solid ratio and the volatilisation of free water and absorbed water in aluminosilicate gel phases were the main reasons for the mass loss in AAMK paste [11]. AAS paste shows the largest mass loss of roughly 16.21% compared to AAF and AAMK pastes, which can be ascribed to the volatilisation of both physically absorbed and chemically bonded water. With the increase of temperature until 550 °C, AAS exhibits a gradual mass loss (3.75% more than PCC), while PCC experiences a rapid mass loss at 450 °C due to the dehydration of Ca(OH)$_2$ [11]. As mentioned in Section 4.1.1, AAS has less thermal stability compared to AAF due to the high calcium content, leading to the formation of additional hydrated phases. Furthermore, a sudden mass loss of AAS paste can be found at around 800 °C, corresponding to the decomposition of calcite [195]. For AAFS paste, the sensitivity of mass loss to high temperatures is dependent on the incorporation of slag. The increase of slag content in AAFS paste can result in an increase of the mass loss [33]. Thus, not all the alkali-activated materials can possess better thermal resistance than PCC in terms of mass loss (which is around 12.46%) and the choice of precursor can significantly affect the thermal stability of AAC at elevated temperatures.
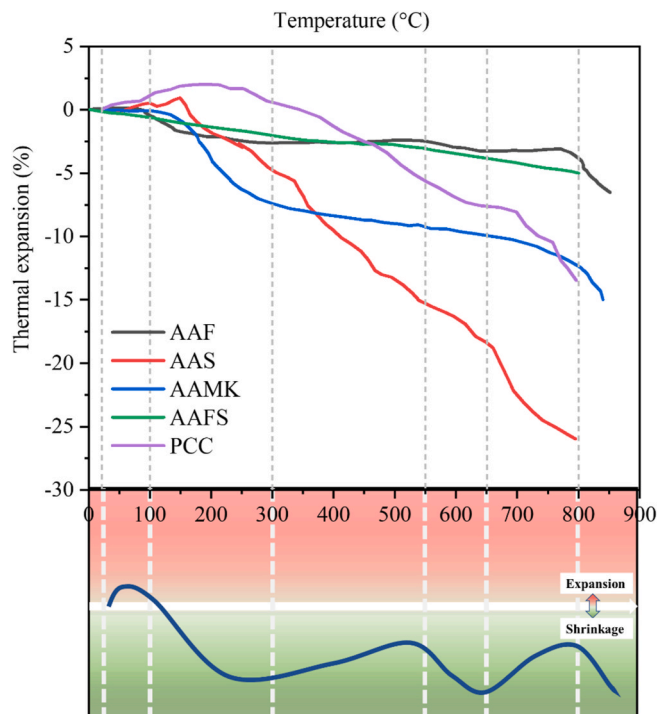
5.2. Thermal deformation

At elevated temperatures, the thermal deformation of AAC needs to be considered, which can influence the thermal compatibility among different phases in AAC. As per previous studies [39,196–198], the thermal expansion of AAF consists of a few stages, as illustrated in Fig. 9. From ambient temperature to around 100 °C, there is a slight expansion in AAF due to water evaporation. At 100–300 °C, a capillary shrinkage takes place, corresponding to the dehydration of AAF matrix. At 300–550 °C, the contraction of AAF matrix continues. As the temperature rises to around 650 °C, viscous sintering can consume fly ash particles in AAF, leading to densification and thus shrinkage of matrix [23]. After 800 °C, the collapse of AAF matrix can be detected. Compared to sodium-based AAF, potassium-based AAF exhibits lower mass loss and volumetric shrinkage due to the higher content of amorphous phase [91]. AAF shows relatively better thermal stability without significant mass loss compared to other types of AAC such as AAS and AAFS, which can be attributed to the stable gel structure with relatively low calcium content as mentioned before [23,39].

For AAS, a slight thermal expansion can be observed from ambient to 150 °C, which is similar to that of AAF, followed by thermal contraction until 800 °C. A relatively significant thermal shrinkage of more than 25% can be detected in AAS, resulting from the thermal incompatibility and aforementioned phase transformation within AAS matrix, which is around 8 times greater than the thermal shrinkage of AAF at 800 °C [121]. AAMK exhibits a less significant thermal contraction of approximately 13% at 800 °C compared to AAS, which can be attributed to the capillary strain, dehydroxylation reactions and sintering and densification effects after exposure to 105–800 °C [124].

In the blend precursor systems, AAFS with 50% slag has a similar thermal strain of roughly 4% in comparison with that of AAF after exposed to 800 °C due to the inclusion of slag that leads to a greater thermal shrinkage [141]. For alkali-activated fly ash-metakaolin pastes, the similar thermal deformation can be detected compared to AAF, where a sharp shrinkage takes place at 100–300 °C. Contrarily, a slight
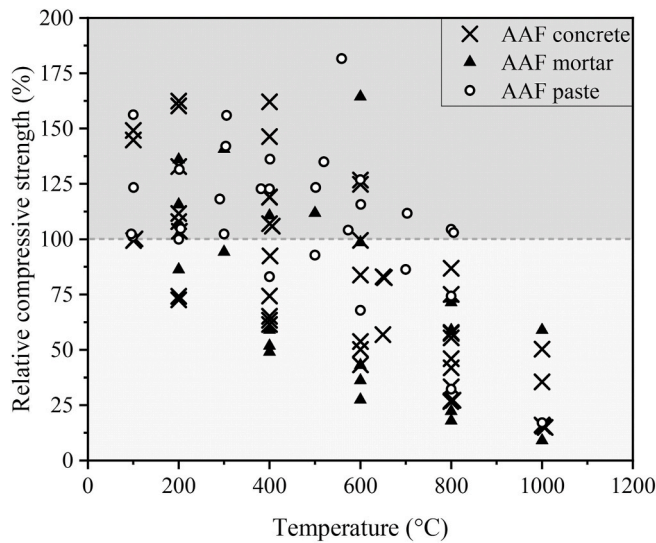
Fig. 10. Relative compressive strength of AAF paste [25,28,29,36,88,104], mortar [26,85,88,91,94,132,151] and concrete [27,32,85–87,90,93,99,129] at elevated temperatures.

thermal expansion can be observed in alkali-activated fly ash-metakaolin mortars from ambient temperature to 800 °C, which can be ascribed to the combined effect of both expansion of aggregates and contraction of paste. This can also result in the development of micro-cracks between different phases and thus the microstructural evolution of AAC.

6. Mechanical properties of AAC at elevated temperatures

Mechanical properties are the most crucial properties of AAC at elevated temperatures, which are highly related to microstructural evolution and phase changes. Based on different single and blend precursor types (including fly ash, slag, metakaolin, and a combination of two or three of them), the changes in compressive, tensile and flexural strengths of AAC with exposure temperature and the effects of different factors on thermal/fire-resistance of AAC are reviewed and discussed herein.

6.1. Compressive strength

6.1.1. Single precursor system

In recent years, the compressive strength of AAF after exposure to various temperatures ranging from ambient temperature to 1200 °C has been increasingly studied. A summary of the existing studies on the relative compressive strength (i.e., ratio of residual compressive strength to original compressive strength) of AAF paste, mortar and concrete at various temperatures is presented in Fig. 10. AAF tends to gain strength at elevated temperatures (≤600 °C) due to the inter-connected small pore network that facilitates the release of moisture pressure at heating and further geopolymerisation that activates the unreacted fly ash particles [3]. Sintering reaction also happens at elevated temperatures, which can lead to stronger inter-particle bonding to enhance strength and offset the strength loss induced by crack initiation and propagation or facilitate AAF matrix to accommodate the deformation of aggregates [106,182,199]. After 600 °C, the compressive strength of exposed AAF experiences a moderate or significant decline compared to the unexposed counterpart. The strength loss of AAF paste is lower than that of AAF concrete as the inclusion of aggregates can lead to thermal incompatibility between AAF paste and aggregates in con-crete [28]. At elevated temperatures, AAF matrix tends to experience shrinkage while aggregates undergo expansion, which can thereby cause damage to the microstructure and reduce the compressive strength [28,

105,145].

The type and size of aggregates can affect the compressive strength loss of AAF concrete. The inclusion of basalt and slag based aggregates leads to a strength loss of 58.4% and 64.6% respectively in AAF concrete after exposure, which can be explained by the closeness of the thermal expansion of these aggregates compared to AAF paste and the original strength characteristics of these aggregates, while other types of ag-gregates such as quartz aggregates, expanded clay aggregates, and lightweight aggregates were also used [101,102,129,147,199,200]. Quartz aggregates can cause obvious strength loss due to the large co-efficient of thermal expansion, while expanded clay aggregates with a relative lower thermal expansion and porous structure can help mitigate the strength loss [147,199]. The use of natural lightweight aggregates (e.g., basaltic pumice) can improve the residual compressive strength [25,101,129,147]. Moreover, the smaller size (2–10 mm) of aggregates can cause explosive spalling in AAF concrete at up to 505 °C, whereas about 30% of residual strength still exists for that with larger size (10–20 mm) of aggregates [28]. The high stiffness of aggregates can restrain shrinkage of AAF at elevated temperatures and the induced radial and tangential stresses surrounding the aggregates leads to cracking [201]. As it is hard for smaller aggregates to produce effective aggregate bridging due to lack of shape irregularity, the use of appro-priate aggregate size and various grading of aggregates can help retain the compressive strength of AAF after exposure to high temperatures.

Apart from aggregate, the mix proportion of AAF paste can also affect the mechanical performance of AAF concrete at elevated temperatures where Si/Al ratio is one of the most crucial factors. AAF concrete with a higher Si/Al ratio (2.2) performs much better than that with a lower Si/Al ratio (1.7) [103], and thus raising the Si content in alkali-activated mixtures is recommended. In addition, the Si/Al ratio ranging from 2.0 to 3.0 can promote strength loss by up to 80%, whereas a ratio of less than 2.0 is more optimal with a 132% strength increase compared to the unexposed specimen [202]. This indicates that Si/Al ratio is a critical parameter in alkali-activated formulations, which needs to be tailored for AAF to achieve a desirable compressive strength after exposure [3]. Other factors (e.g., curing condition) can also affect the change of compressive strength of AAF at elevated temperatures. The experi-mental study on the effect of ambient and heat curing on the mechanical properties of AAF after high-temperature exposure indicated that the ambient-cured AAF concrete experienced lower strength deterioration than the heat-cured one after exposed to 1000 °C [27]. Thus, the residual
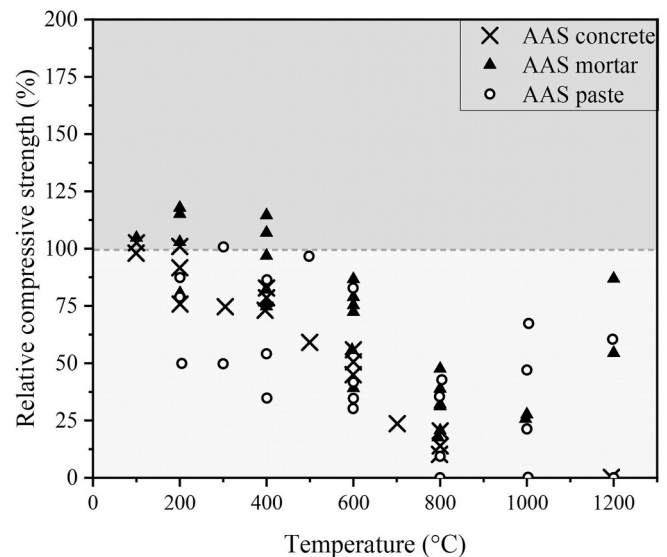

Fig. 11. Relative compressive strength of AAS paste [26,37,114,118,119], mortar [113,117,120,131,147,149] and concrete [112,115,121] at elevated temperatures.
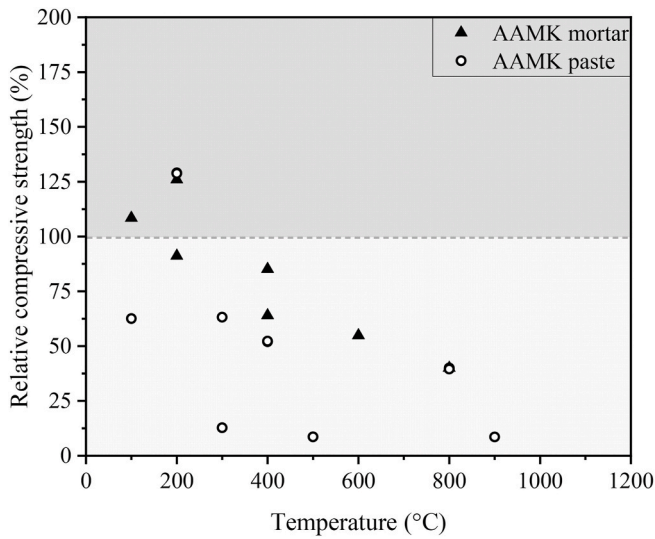
Fig. 12. Relative compressive strength of AAMK paste [36,124–126] and mortar [123,147] at elevated temperatures.

compressive strength of AAF at elevated temperatures is dependent on many factors such as compatible aggregates and optimal alkali-activated formulation.

Fig. 11 displays the relative compressive strength of AAS paste, mortar and concrete at elevated temperatures, indicating that the compressive strengths of AAS paste, mortar and concrete reduce significantly against exposure temperature, where the highest strength loss appears at around 800 °C [26,37,112–115,117–121,131,147,149]. The retention strength ranges from 0 to approximately 50% at this temperature level. This can be attributed to the dehydration of AAS matrix and decomposition of calcite [114]. Some of the specimens exhibit an enhanced compressive strength at 200 °C and 400 °C, which can be mainly ascribed to the acceleration of hydration process by heating, activating the slag particles with strength gain [112,117]. It is noteworthy that after obvious decline of strength at 800 °C, AAS pastes and mortar specimens start to gain strength when the temperature continues to rise until 1000 °C. This can be explained by the densification of AAS matrix during viscous heating, which causes a reduction of voids and thereby enhances the compressive strength [114]. Also, the
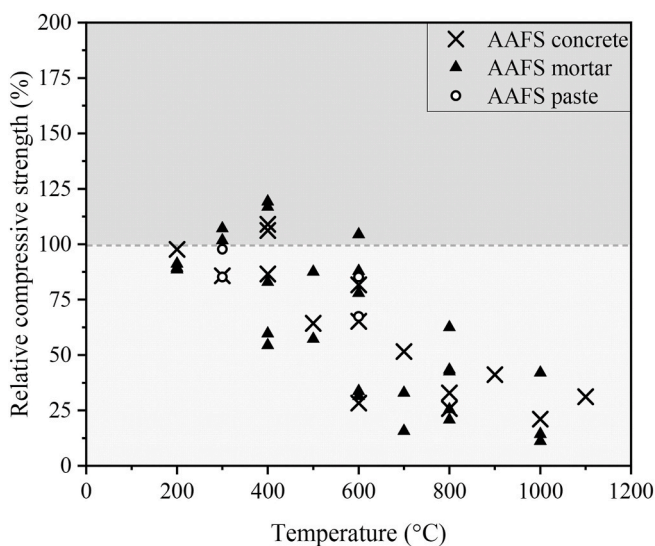
formation of new crystalline phases such as gehlenite and larnite contribute to the densification of AAS after high temperature exposure. Among AAF, AAMK and AAS, AAS tends to have the lowest thermal/fire resistance whereas AAF performs best and thus can be regarded as a good choice in high-temperature resistance applications. This is also consistent with that presented in the previous section that AAF shows the best thermal stability compared to other types of AAC.

Fig. 12 shows the experimental results of relative compressive strength of AAMK paste and mortar as a function of exposure temperature collected from literature [36,123–126,147], indicating that AAMK possesses a dense and homogeneous microstructure without prominent pore structure evolution at elevated temperatures [36]. Thus, the moisture is prone to be trapped inside the dense pore structure, leading to the accumulation of pore pressure and thus a significant strength reduction. Most results of the relative compressive strength are below 100% at elevated temperatures ranging from 100 °C to 900 °C, suggesting that the compressive strength of AAMK after exposure is retained or gained less than that of AAF. This is because sintering reaction takes place in AAF matrix at elevated temperatures, which can rearrange the pore structure with evolution of pores with large size to smaller ones. A large number of small pores can provide channels for free water and vapour to escape without pore pressure build-up [36,203], while metakaolin-based AAC matrix tends to have a higher moisture content with a denser pore structure compared to AAF, which would be subjected to a higher risk of pore pressure induced damage at elevated temperatures [3].

6.1.2. Blend precursor system

Fig. 13 presents a summary of the relative compressive strength of AAFS paste, mortar and concrete at elevated temperatures, indicating a similar change trend as that for AAS system, with a slight increase of residual strength after exposure to 200–600 °C. The most essential factor that affects the mechanical behaviour of AAFS at elevated temperatures is the fly ash/slag ratio. The effect of fly ash/slag ratio by weight on relative compressive strength of AAFS is depicted in Fig. 14. AAF concrete and AAS concrete have the highest and lowest retention strength at up to 600 °C, respectively, while the residual strength of AAFS concrete is in between those two. Moreover, the increase of initial strength could lead to a more significant strength loss after exposure as the slag content increases from 0 to 100% [3,139]. Ductility of AAFS matrix is a governing factor in the level of thermal incompatibility induced damage. AAFS matrix with higher ductility can better accommodate the thermal shrinkage and expansion occurred in different phases and thus reduce
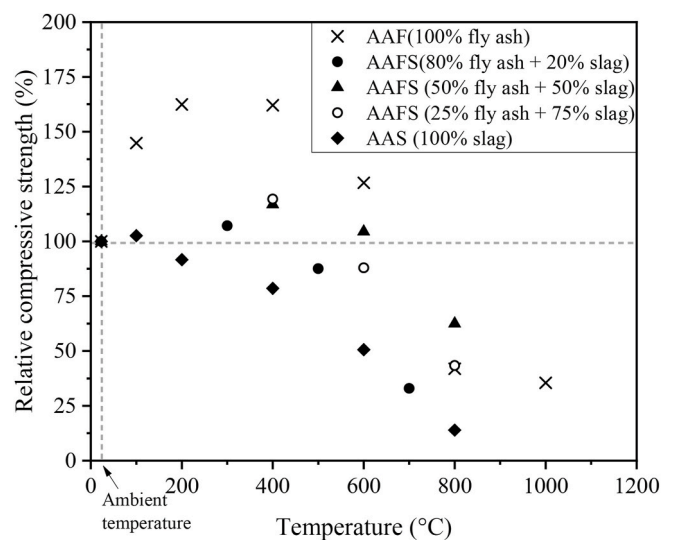

Fig. 13. Relative compressive strength of AAFS paste [26], mortar [26,33,131, 132,137] and concrete [133,135,136,138].

Fig. 14. Effect of fly ash/slag ratio on the relative compressive strength of AAF [27], AAFS [33,126] and AAS [101] concrete at elevated temperatures.
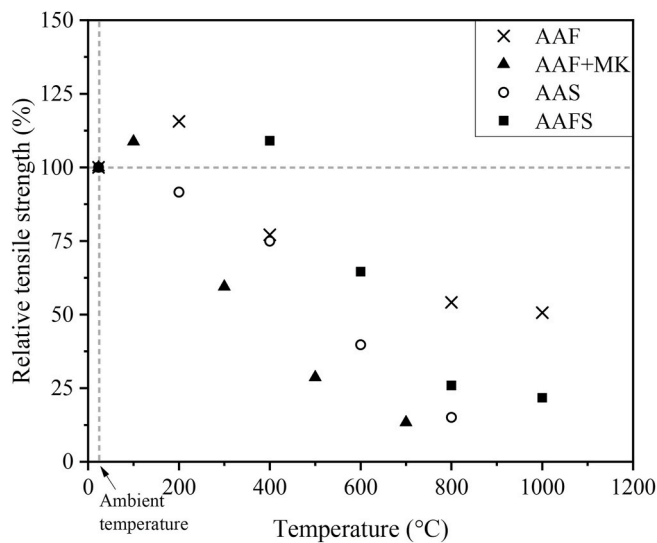
Fig. 15. Relative tensile strength of AAC at elevated temperatures [86,97,116, 133,145].
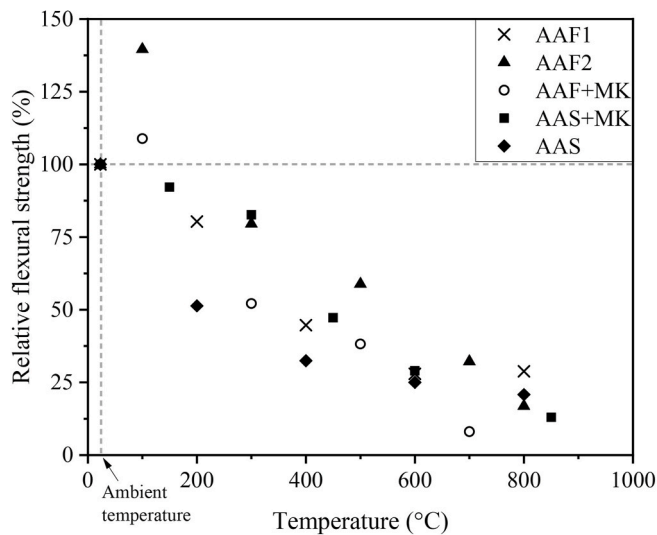

Fig. 16. Relative tensile strength of AAC at elevated temperatures [36,94,113, 145,148].

the compressive strength loss after exposure to high temperatures [3, 24].

6.2. Tensile strength

Fig. 15 displays the residual tensile strength of AAC obtained from literature [86,97,116,133,145]. Similar to relative compressive strength, AAC containing fly ash including AAF, AAFS and alkali-activated fly ash-metakaolin concrete exhibits a slight enhancement of tensile strength at elevated temperatures until 400 °C. This can be ascribed to the further geopolymerisation that activates the unreacted precursor particles inside the matrix as well as the occurrence of sintering reaction. Without fly ash, the tensile strength of AAS declines continuously, which is consistent with the compressive strength change with exposure temperature. A combined effect of further geo-polymerisation and thermal incompatibility is regarded as the cause for the tensile strength drop at elevated temperatures, similar to the compressive performance.

Table 3
Effect of Si/Al ratio on mechanical properties of AAC at elevated temperatures.

Ref.	Precursor	Si/Al ratio	Main findings
[103]	Fly ash	1.7–2.2	The residual strength of samples with Si/Al ratio of 2.2 is the highest.
[182]	Fly ash	1.2–8.8	The residual strength of AAC with Si/Al ratio of 1.2 is 18% at 1000 °C, whereas it is 400% for AAC with Si/Al ratio of 8.8 at 1000 °C.
[124]	Metakaolin	1.03–2.00	The highest strength (6 MPa which is about 9% of the original strength) occurs when Si/Al ratio is 1.75, whereas it is 0% for samples with Si/Al ratio of 1.03.
[202]	Fly ash	<2	The use of low Si/Al ratio (<2) can result in a 132% increase of compressive strength after exposure of 1000 °C.
[205]	Fly ash	1–3	The AAF gel with Si/Al ratio of 2 exhibits superior performance compared to those with lower Si/Al ratio.

6.3. Flexural strength

The relative flexural strength of different types of AAC at elevated temperatures is illustrated in Fig. 16. A similar tendency can be observed for tensile and flexural strengths of AAC at elevated temperatures. In comparison with compressive strength, flexural strength is more sensitive to the initiation and propagation of micro-cracks inside AAC matrix [195]. Therefore, the micro-cracks induced by matrix shrinkage when exposed to high temperatures can cause a radial drop in flexural strength of AAC [117], as seen from all specimens in Fig. 16. Moreover, the microstructural evolution (e.g., pore structure characteristic changes) can significantly affect the flexural strength degradation at elevated temperatures [145]. The large number of small pores distributed in AAF can accommodate the pore pressure induced by heating to reduce the flexural strength loss, while other types of AAC may show a more rapid decline when the exposure temperature rises.

7. Approaches to mitigating damage of AAC at elevated temperature

7.1. Modification of AAC

7.1.1. Tailoring precursors

As discussed above, the mechanical properties of AAC at elevated temperatures can be affected by different factors, among which Si/Al is one of the critical factors. Table 3 summarises the relevant studies on the effect of Si/Al ratio on mechanical properties of AAC. It is indicated that a higher Si/Al ratio can lead to a better residual strength of AAC after exposed to high temperatures. As the Si/Al ratio rises from 1.2 to 8.8, the residual strength of AAC is improved from 18% to around 400% of the original strength at 1000 °C [182]. This can be mainly explained by the fact that the higher Si content can result in higher conversion of fly ash particles into amorphous aluminosilicate alkali-activated gel [39,103]. The formation of aluminosilicate improves the internal pore/void connectivity of AAC, mitigating the vapour pressure accumulation due to pore pressure release through the interconnected pore network [39]. Thus, the pore pressure induced damage is mitigated and the residual strength is increased. Furthermore, the increase of Si/Al ratio can lead to the rise in initial temperature of gel crystallisation [204]. A range of Si/Al ratio of 1–3 was generally studied in literature. It was found that higher Si/Al ratio resulted in superior performance of AAF and AAMK after exposed to high temperatures [39,103,124,182,202,205], implying the importance of Si/Al ratio to AAC mix design.

7.1.2. Incorporating additives

To improve the mechanical behaviour of AAC at elevated temperatures, some additives such as quartz and silica fume are used to maintain

the dimensional stability of AAC and increase the Si/Al ratio [39,96, 103]. The increase of quartz powder dosage (up to 30%) can lead to a higher degree of reactivity and sintering in AAF at 1000 °C and thus enhance the residual strength of the matrix [96]. The incorporation of fine filler particles such as silica powder and ceramic powder into AAC can reduce the thermal shrinkage and thus improve the residual strength after exposed to high temperatures [39,96]. AAMK containing fine ceramic powders can achieve a higher compressive strength at 1000 °C, as the addition of fine particles can improve the pore size and shape distribution while filling the gap between large aggregates [39,206]. As ceramic powder exhibits good volume stability, an effective barrier can be formed inside the matrix to mitigate the thermal stress induced damage [206]. The thermal shrinkage can be effectively improved, and thus the damage mechanism associated with thermal incompatibility can be tackled. However, the additives do not always benefit AAC. For instance, silica fume was found to have a negative impact on AAC at elevated temperatures in some cases [71,207,208]. AAMK containing silica fume has a lower residual strength compared to the plain specimens after exposure to 800 °C, while reversed results can be observed at ambient temperature [71]. This can be ascribed to the denser internal structure of AAMK after adding silica fume, which impedes the escape of vapour pressure and thus deteriorate the pore pressure induced damage [1]. Hence, it is crucial to select the appropriate additives and precursor type for mitigating the damage of AAC at elevated temperatures.

7.1.3. Adopting appropriate aggregates

Aggregate is an essential phase for AAC. The commonly used aggregates can be divided into two categories: conventional aggregates and recycled aggregates [39]. The conventional aggregates include carbonate aggregates (specific heat between 150 °C and 400 °C) and siliceous aggregates (specific heat at about 500 °C) [68,209,210]. Carbonate aggregates have a 10 times greater heat absorption capacity than siliceous aggregates after exposure to 600 °C, which can be attributed to the emission of carbon dioxide from the decomposition of carbonate at high temperatures [39]. The effects of different types of aggregates on the thermal behaviour of AAC discussed in Section 6.1.1 suggest that the use of some appropriate aggregates (e.g., expanded clay aggregates) can mitigate the thermal incompatibility between different phases in AAC and thus the damage at elevated temperatures.

Recycled aggregates such as recycled ceramic aggregates, crumb rubber and glass waste have been increasingly adopted to tackle the environmental issue of industrial wastes. The use of recycled ceramic aggregates can negatively affect the flowability of concrete at ambient temperature, whereas they have a negligible effect on the compressive strength of concrete with a slight improvement after exposed to 800 °C [211]. The addition of crumb rubber can reduce the residual strength of concrete by around 30% and 25% compared to the plain concrete at room temperature and 600 °C, respectively [212]. Glass wastes have high fire-resistant capacity and thus can benefit concrete after exposed to 600 °C as the molten glass can fill the microcracks in the matrix induced by pore pressure and thermal gradient to prevent crack growth

Table 4
Physical and thermal properties of fibres for AAC [57,125,214–223].

Fibre type	Tensile strength (MPa)	Young's modulus (GPa)	Elongation ratio (%)	Specific gravity	Melting point (°C)
Steel	200–2760	200	0.5–35	7.8	1370
PP	552–690	3.45	~25	0.9	170
PVA	1000–1600	22–42	6–7	1.3	220–240
PE	~690	0.14–0.41	~10	0.95	141.4
Glass	1034–3792	72	1.5–3.5	2.5–2.7	860
Basalt	872–2800	40–89	3.15	2.8	1500–1700
Carbon	1550–6960	159–965	2.5–3.2	1.8	Over 3000
Nylon	750–1000	2.5–5.17	15–30	1.14	231–252
Jute	400–800	13–26.5	1.8	1.3–1.45	–

Table 5
A summary of behaviour of steel fibre reinforced concrete (SFRC) at elevated temperatures.

Ref.	Replacement material	Dimension of fibre		Volume fraction (%)	Main findings
		Length (mm)	Diameter (μm)		
[231]	Fly ash, silica fume	25	417	0, 1	Heating up to 800 °C, SFRC has 55% more residual strength compared to the plain one.
[79]	Fly ash, silica fume	25	417	0, 1	After exposed to 1100 °C, SFRC has a 76% increase of residual strength.
[74]	Fly ash	60	900	0.5, 0.75	SFRGC showed higher residual strength than PCC. The original temperature is retained until 400 °C.
[68]	Fly ash	25	500	0, 1, 3	Steel fibres improved the tensile strength via crack-bridging at elevated temperatures.
[218]	Fly ash	13	160	0, 0.5	Steel fibres had almost no effect on the permeability of concrete at 20–300 °C.
[232]	Fly ash, silica fume	30	600	0, 0.5	Steel fibres improved the residual strength up to 300 °C but spalling could not be prevented.
[63]	Fly ash, slag	38	114	0, 0.5	The addition of steel fibres did not obviously affect the compressive strength at 800 °C.
[229]	Fly ash, slag, silica fume	60	750	0–1	The residual tensile strength of SFRC (optimal 0.75%) is much greater than that of PFRC.
[228]	Slag, silica fume	13.2	220	0, 1, 2, 3	A higher content (3%) of steel fibres could not enhance the residual compressive strength.
[61]	Slag	32.6	950	0–2	The addition of slag and steel fibres (optimal 1%) improved splitting strength of concrete.
[71]	Metakaolin, silica fume	25	417	0, 1	The addition of steel fibres greatly improved the toughness at elevated temperatures.

[213]. The use of recycled aggregates can generally enhance the fire-resistance of concrete, while the type and dosage of them need to be considered to maintain the fresh properties of AAC at room temperature and mechanical performance at elevated temperatures.

7.2. Incorporation of fibres

The addition of fibres is another important approach to mitigating damage in concrete at elevated temperatures. As seen in Table 1, the existing studies on the behaviour of fibre reinforced AAC are very limited. It was reported that the incorporation of fibres can extend the plastic deformation of concrete and thus influence the failure patterns [1,39]. The commonly used fibres include steel, synthetic (e.g., polypropylene (PP), polyvinyl alcohol (PVA) and polyethylene (PE)), glass, basalt, carbon and natural fibres, the physical and thermal properties of which are summarised in Table 4 [1,39]. Here, special focus is placed on steel fibre, PP fibre and hybrid fibre composed of them.

7.2.1. Steel fibres

Steel fibres are widely adopted for PCC because of their excellent mechanical performance, flexibility and availability [224]. Steel fibre reinforced concrete (SFRC) can achieve higher tensile strength, toughness, strain and energy absorption capacity and better impact resistance compared to plain concrete [1,225,226]. Due to their high melting point and strong thermal stability, the residual strength of fibre-reinforced concrete can be retained at a certain level [1,39,93]. The studies on steel fibre-reinforced concrete containing different supplementary cementitious materials are summarised in Table 5. At ambient temperature, the increase of steel fibre content from 1% to 3% can result in the enhancement of compressive strength of concrete [227,228]. After exposed to high temperatures, the effect of steel fibre in concrete varies with different aspects such as fibre dosage and temperature level [1,26, 39]. There exists a positive relation between compressive strength of concrete at 400 °C and steel fibre dosage (from 0% to 1%), whereas an opposite impact appears after exposed to 600 °C [41,229]. However, concrete reinforced with 1–2% steel fibres can improve the residual compressive strength of concrete compared to plain concrete at up to 1000 °C, indicating that temperature-induced damage can be effectively mitigated through the incorporation of steel fibres [39,42,153].

Moreover, the incorporation of steel fibres was found to effectively improve the residual tensile strength of concrete due to their high tensile strength. At ambient temperature, SFRC has better tensile strength and strain capacity compared to plain concrete, which can be attributed to the fibre bridging effect [68,230]. The tensile strength reduction of SFRC is slower than that of plain concrete from ambient temperature to around 400 °C due to the high thermal conductivity of steel fibres that can transmit heat through concrete from the heated side to the cold side more homogeneously in SFRC. Thus, the thermal stress-induced damage can be mitigated with a more uniform temperature profile at the early stage of heating [42]. However, the strength loss can be increased more rapidly when the temperature exceeds 400 °C until 800 °C is reached [226]. Compared to plain concrete, SFRC has around 48% and 41% more residual strength after exposed to 400 °C and 600 °C, respectively [1,226]. Regarding the effect of steel fibre content on tensile behaviour of concrete at elevated temperatures, for SFRC containing 10% slag, the optimal fibre content was found to be 3% with the best residual tensile strength compared to those with 1–2% of steel fibre after exposure to 800 °C while 1% of steel fibre addition showed better performance in residual tensile strength at 400 °C for concrete with 40% slag [226]. Regarding the application of steel fibres in AAC at elevated temperatures, there are only few preliminary studies on the physical and mechanical performance of AAF. AAF with 1.5% steel fibre dosage exhibited a 15.4% and 13.07% strength gain compared to plain AAF at ambient temperature and after exposure to 800 °C, respectively [111]. However, the research on the effect of steel fibres on different types of AAC in terms of phase stability, pore structure and microstructural

Table 6
A summary of behaviour of PP fibre reinforced concrete (PFRC) at elevated temperatures.

Ref.	Replacement material	Dimension of fibre		Volume fraction (%)	Main findings
		Length (mm)	Diameter (μm)		
[231]	Fly ash, silica fume	19	53	0, 0.22	After 800 °C, PFRC had a 4.4% strength reduction compared to the control sample.
[79]	Fly ash, silica fume	19	53	0, 0.22	Heating up to 1100 °C, the addition of PP fibres helped with the strength retention.
[232]	Fly ash, silica fume	30	–	0, 0.05	The spalling resistance of HPC was increased with the addition of PP fibre, whereas the residual strength slightly suffered from that.
[233]	Fly ash, silica fume	3–30	40	0, 0.05, 0.1, 0.15	The effectiveness of PP fibre was dependent on the melting point, fibre length and volume.
[234]	Fly ash	19	70	0.05, 0.1	When the volume fraction of PP fibre was more than 0.05%, the spalling was resisted.
[235]	Fly ash	19	–	0, 0.05, 0.1, 0.15	The optimal volume fraction of PP fibre was found to be 0.05%.
[63]	Fly ash, slag	20	–	0, 0.11	The PP fibre could reduce the residual tensile strength of concrete without an obvious effect on compressive strength.
[236]	Fly ash, slag	20		0, 0.11	Both specimens with and without PP fibres experienced strength degradation.
[61]	Slag	19	–	0–0.133	The optimal dosage of PP fibre was 1%.
[229]	Fly ash, slag, silica fume	65	850	0–0.2	The residual strength was around 20% for specimens with PP fibres after exposed to 900 °C.

evolution at high temperatures is lacking.

7.2.2. Synthetic fibres

Synthetic fibres are mainly produced from raw industrial materials or recycled from plastic wastes. The addition of recycled polymer fibres in concrete can provide a sustainable and feasible solution for the consumption of disposed plastics which can cause environmental pollution
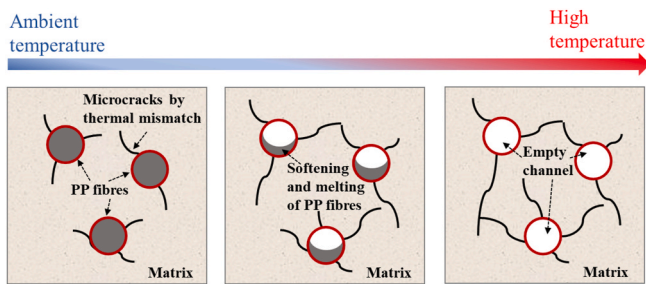
Fig. 17. Schematic illustration of microstructural evolution of PP fibre reinforced concrete at elevated temperatures.

[224]. The most commonly used synthetic fibres include PP, PVA, PE and PET fibres. Among them, PP is commonly used to reduce the high temperature-induced damage and prevent spalling [1,40]. Some relevant studies on the behaviour of PP fibre reinforced concrete (PFRC) are briefly summarised in Table 6.

Unlike steel fibres that have a strong thermal stability, PP fibres have a relatively low melting point of around 170 °C. Thus, the mechanism of using PP fibres to improve the thermal performance of concrete is associated with the expansion and melting of fibres in concrete matrix. Fig. 17 schematically illustrates the microstructural evolution of PFRC at elevated temperatures. It was reported that the residual strength of concrete reinforced with 0.17% PP fibres went up first until 350 °C, followed by a slight drop between 350 °C and 450 °C and a significant decline after 450 °C [4]. This is because at the early stage of heating, the matrix might not be influenced by the addition of PP fibre while the further hydration of cement paste or geopolymerisation in AAC with the increase of temperature can lead to strength gain for concrete [229, 237]. Compared to plain concrete, the incorporation of PP fibres was found to improve the residual compressive strength by up to 13% when the temperature was increased from 400 °C to 600 °C [42]. The enhancement of residual strength is because of the coefficient of thermal expansion of PP fibres, which is around 10 time greater than that of other phases in concrete. This leads to the initiation of multiple microcracks that can improve the interconnection between pores and thus provide the pathways for vapour pressure to escape and prevent pore pressure accumulation [2,47,157]. The length of PP fibres can also affect the compressive strength of PFRC. When the fibre length increased from 6 mm to 12 mm, the residual strength can be slightly improved by about 4% after exposed to 600 °C [42]. PP fibres should be large enough to have a better dispersion in concrete [65].

Besides the compressive strength, the addition of PP fibres can enhance the residual splitting tensile strength of concrete [238–241]. Compared to plain concrete, PFRC has around 27% more retained tensile splitting strength at elevated temperatures [240]. Nevertheless, the effect of PP fibres on the residual tensile strength is dependent on the matrix proportions, fibre content and fibre length. PP fibres with 12 mm length perform better on mitigating the tensile loss in PFRC compared to those with 6 mm length [42,240].

7.2.3. Hybrid fibres

To combine the advantages of different types of fibres, hybrid fibre reinforced concrete has been increasingly studied. For instance, steel fibres are used to restrict the initiation and propagation of microcracks together with PP fibres that can improve the internal connectivity of concrete, and thus can enhance the thermal behaviour of concrete at elevated temperatures. The residual compressive strength of hybrid steel and PP fibre reinforced concrete was higher than that of plain concrete at temperatures between 20 °C and 300 °C [59]. Concrete reinforced with 1% steel and 0.22% PP fibres showed a relatively greater compressive strength retention than PFRC while worse than SFRC when exposed to 800 °C [71], as PP fibres have a much lower melting point than steel fibres and lose strength quickly when the melting point of

around 170 °C is achieved while steel fibres have a better thermal stability to function properly when the temperature continues to rise [1]. A hybrid of high tensile strength fibres (e.g., steel fibres and carbon fibres) and low melting point fibres (e.g., PP and PVA fibres) can maximise the damage mitigation effect in concrete at high temperatures, where hybrid steel and PP fibre reinforced concrete exhibits the most superior mechanical behaviour [1]. In regard to AAC at elevated temperatures, a combination of glass and basalt fibres was employed to mitigate the compressive and flexural strength losses of AAF at elevated temperatures, where glass fibres provided superior bonding and bridging effect due to less agglomerated distribution [108]. The feasibility of using steel, PP and hybrid fibres to mitigate the damage in AAC at elevated temperatures has been rarely studied and thus further research from the microscopic and macroscopic points of view is required to understand the behaviour of hybrid fibre reinforced AAC at elevated temperatures.

8. Conclusions and perspectives

8.1. Conclusions

Herein, a critical literature review on the behaviour of single precursor and blend precursor AAC systems at elevated temperatures and some approaches to mitigating the damage of AAC subjected to high temperatures was carried out, aiming to gain an in-depth insight of the underlying mechanisms and identify potential areas for further research to develop AAC with desirable resistance to elevated temperatures and fire. The main conclusions can be drawn: (1) The damage mechanisms of AAC at elevated temperatures can be summarised in three aspects: thermal-induced damage due to phase incompatibility between matrix and aggregates, pore pressure-induced damage due to vapour pressure build-up, and phase transformation during the heating process. (2) For the single precursor systems, the formation of new crystalline phases including albite and nepheline takes place in AAF after exposure to more than 300 °C, along with the increased pore size and volume. AAF tends to gain compressive strength after exposed to more than 600 °C due to the interconnected small pore network and further geopolymerisation that activates the unreacted fly ash particles. At 800 °C, the sintering effect and densification occurs in AAF matrix with a more compact microstructure, leading to the reduction of high temperature-induced strength loss. In general, AAF has superior residual tensile and flexural strengths compared to other types of AAC at elevated temperatures. (3) Compared to AAF, there are additional hydrated phases in AAS due to the relatively higher calcium content, reducing the thermal resistance and stability of AAS matrix. The dehydration of reaction products happens at a temperature level of 200–600 °C. The highest compressive strength loss appears at around 800 °C for AAS due to the dehydration of AAS matrix and decomposition of $CaCO_3$. (4) Regarding the blend precursor systems, AAFS with lower slag content (10–20% by weight) contains the similar crystalline phases as found in AAF, including quartz and mullite, while the C–S–H phase exists in AAFS when the slag content reaches 40–50%. The slag content has a significant influence on the microstructural characteristics and macroscopic properties of AAFS at elevated temperatures. (5) To enhance the high-temperature resistance, modification of AAC matrix with a higher Si/Al ratio can lead to better residual strength of AAC after exposure by tackling pore pressure-induced damage. The incorporation of fine filler particles can reduce the thermal shrinkage and thus improve the residual strength of AAC. Employing steel fibres (0–3% by volume) can enhance the thermal properties of concrete, attributing to their high melting point and strong thermal stability. The addition of PP fibres (0–0.22% by volume) can mitigate pore pressure-induced damage, as they have a relatively low melting point that provides inter-connected channels to release accumulated pressure. The hybrid steel and PP fibres have an obvious effect on mitigating the concrete damage at elevated temperatures as steel fibres can restrict the initiation of microcracks while PP fibres can increase the internal connectivity of matrix.

8.2. Perspectives

Driven by the need to further investigate high-temperature resistance and improve thermal properties of AAC, some challenges can be addressed for future research. (1) A systematic study on the effects of different factors such as precursor content, alkaline activator type and curing condition on the reaction kinetics, microstructure and macroscopic properties of blended AAC systems at elevated temperature from a multiscale point of view is required to optimise the mix proportions of AAC with desirable high-temperature/fire resistance. (2) More efforts are needed to find or develop novel sustainable additives for enhancing high-temperature/fire resistance of AAC without compromising mechanical properties, where the recycled materials and industrial wastes can be considered. (3) For better enhancing the thermal behaviour of AAC, the feasibility and effectiveness of incorporating different types of fibre (including those recycled from end-of-life products) in AAC subjected to high temperatures can be explored. (4) Multiscale modelling can be employed to explore the damage evolution as a complement to experimental studies and thus gain in-depth insights into the behaviour of AAC at elevated temperatures.

Declaration of competing interest

The authors declare that they have no known competing financial interests or personal relationships that could have appeared to influence the work reported in this paper.

Data availability

Data will be made available on request.

Acknowledgements

References

[1] H.Y. Wu, X.S. Lin, A.N. Zhou, A review of mechanical properties of fibre reinforced concrete at elevated temperatures, Cement Concr. Res. 135 (2020), 106117.

[2] Y. Li, P. Pimienta, N. Pinoteau, K.H. Tan, Effect of aggregate size and inclusion of polypropylene and steel fibers on explosive spalling and pore pressure in ultra-high-performance concrete (UHPC) at elevated temperature, Cement Concr. Compos. 99 (2019) 62–71.

[3] M.K. Lahoti, K.H. Tan, E.H. Yang, A critical review of geopolymer properties for structural fire-resistance applications, Construct. Build. Mater. 221 (2019) 514–526.

[4] T. Drzymala, W. Jackiewicz-Rek, M. Tomaszewski, A. Kus, J. Galaj, R. Sukys, Effects of high temperature on the properties of high performance concrete (HPC), modern building materials, Struct. Tech. 172 (2017) 256–263.

[5] I. Niklioc, S. Markovic, I. Jankovic-Castvan, V.V. Radmilovic, L. Karanovic, B. Babic, V.R. Radmilovic, Modification of mechanical and thermal properties of fly ash-based geopolymer by the incorporation of steel slag, Mater. Lett. 176 (2016) 301–305.

[6] M. Chen, Z. Sun, W. Tu, X. Yan, M. Zhang, Behaviour of recycled tyre polymer fibre reinforced concrete at elevated temperatures, Cement Concr. Compos. (2021), 104257.

[7] W.L. Tu, Y. Zhu, G.H. Fang, X.G. Wang, M.Z. Zhang, Internal curing of alkali-activated fly ash-slag pastes using superabsorbent polymer, Cement Concr. Res. 116 (2019) 179–190.

[8] Z.G. Shi, C.J. Shi, J. Zhang, S. Wan, Z.H. Zhang, Z.H. Ou, Alkali-silica reaction in waterglass-activated slag mortars incorporating fly ash and metakaolin, Cement Concr. Res. 108 (2018) 10–19.

[9] J.L. Provis, Alkali-activated materials, Cement Concr. Res. 114 (2018) 40–48.

[10] J.L. Provis, A. Palomo, C.J. Shi, Advances in understanding alkali-activated materials, Cement Concr. Res. 78 (2015) 110–125.

[11] O.G. Rivera, W.R. Long, C.A. Weiss, R.D. Moser, B.A. Williams, K. Torres-Cancel, E.R. Gore, P.G. Allison, Effect of elevated temperature on alkali-activated geopolymeric binders compared to portland cement-based binders, Cement Concr. Res. 90 (2016) 43–51.

[12] R.D. Moser, P.G. Allison, B.A. Williams, C.A. Weiss, A.D. Diaz, E.R. Gore, P.G. Malone, Improvement in the geopolymer-to-steel bond using a reactive vitreous enamel coating, Construct. Build. Mater. 49 (2013) 62–69.

[13] G.H. Fang, W.K. Ho, W.L. Tu, M.Z. Zhang, Workability and mechanical properties of alkali-activated fly ash-slag concrete cured at ambient temperature, Construct. Build. Mater. 172 (2018) 476–487.

[14] F. Colangelo, I. Farina, M. Travaglioni, C. Salzano, R. Cioffi, A. Petrillo, Eco-efficient industrial waste recycling for the manufacturing of fibre reinforced innovative geopolymer mortars: integrated waste management and green product development through LCA, J. Clean. Prod. 312 (2021), 127777.

[15] F. Xu, G.H. Gu, W. Zhang, H.M. Wang, X.M. Huang, J. Zhu, Pore structure analysis and properties evaluations of fly ash-based geopolymer foams by chemical foaming method, Ceram. Int. 44 (2018) 19989–19997.

[16] A. Hassan, M. Arif, M. Shariq, Use of geopolymer concrete for a cleaner and sustainable environment - a review of mechanical properties and microstructure, J. Clean. Prod. 223 (2019) 704–728.

[17] J.H. Zhao, L.Y. Tong, B.E. Li, T.H. Chen, C.P. Wang, G.Q. Yang, Y. Zheng, Eco-friendly geopolymer materials: a review of performance improvement, potential application and sustainability assessment, J. Clean. Prod. 307 (2021), 127085.

[18] D.L. Kong, J.G. Sanjayan, K. Sagoe-Crentsil, Comparative performance of geopolymers made with metakaolin and fly ash after exposure to elevated temperatures, Cement Concr. Res. 37 (2007) 1583–1589.

[19] A. Hassan, M. Arif, M. Shariq, T. Alomayri, S. Pereira, Fire resistance characteristics of geopolymer concrete for environmental sustainability: a review of thermal, mechanical and microstructure properties, Environ. Dev. Sustain. (2022) 1–36.

[20] T. Luukkonen, Z. Abdollahnejad, J. Yliniemi, P. Kinnunen, M. Illikainen, One-part alkali-activated materials: a review, Cement Concr. Res. 103 (2018) 21–34.

[21] T.W. Cheng, J.P. Chiu, Fire-resistant geopolymer produced by granulated blast furnace slag, Miner. Eng. 16 (2003) 205–210.

[22] A. Buchwald, M. Hohmann, C. Kaps, H. Bettzieche, J.T. Kuhnert, Stabilised foam clay material with high performance thermal insulation properties, Cfi-Ceram Forum Int 81 (2004) E39–E42.

[23] Y. Luo, S.H. Li, K.M. Klima, H.J.H. Brouwers, Q.L. Yu, Degradation mechanism of hybrid fly ash/slag based geopolymers exposed to elevated temperatures, Cement Concr. Res. 151 (2022), 106649.

[24] Z. Pan, J.G. Sanjayan, B.V. Rangan, An investigation of the mechanisms for strength gain or loss of geopolymer mortar after exposure to elevated temperature, J. Mater. Sci. 44 (2009) 1873–1880.

[25] Z. Pan, J.G. Sanjayan, F. Collins, Effect of transient creep on compressive strength of geopolymer concrete for elevated temperature exposure, Cement Concr. Res. 56 (2014) 182–189.

[26] Z. Pan, Z. Tao, Y.F. Cao, R. Wuhrer, T. Murphy, Compressive strength and microstructure of alkali-activated fly ash/slag binders at high temperature, Cement Concr. Compos. 86 (2018) 9–18.

[27] H.G. Zhang, L. Li, C. Yuan, Q.Y. Wang, P.K. Sarker, X.S. Shi, Deterioration of ambient-cured and heat-cured fly ash geopolymer concrete by high temperature exposure and prediction of its residual compressive strength, Construct. Build. Mater. 262 (2020), 120924.

[28] D.L.Y. Kong, J.G. Sanjayan, Effect of elevated temperatures on geopolymer paste, mortar and concrete, Cement Concr. Res. 40 (2010) 334–339.

[29] T. Alomayri, L. Vickers, F.U.A. Shaikh, I.M. Low, Mechanical properties of cotton fabric reinforced geopolymer composites at 200-1000 degrees C, J Adv Ceram 3 (2014) 184–193.

[30] G. Humur, A. Cevik, Mechanical characterization of lightweight engineered geopolymer composites exposed to elevated temperatures, Ceram. Int. 48 (2022) 13634–13650.

[31] X. Jiang, Y.Y. Zhang, R. Xiao, P. Polaczyk, M.M. Zhang, W. Hu, Y. Bai, B.S. Huang, A comparative study on geopolymers synthesized by different classes of fly ash after exposure to elevated temperatures, J. Clean. Prod. 270 (2020), 122500.

[32] A. Hassan, M. Arif, M. Shariq, Mechanical behaviour and microstructural investigation of geopolymer concrete after exposure to elevated temperatures, Arabian J. Sci. Eng. 45 (2020) 3843–3861.

[33] F.L. Qu, W.G. Li, Z. Tao, A. Castel, K.J. Wang, High temperature resistance of fly ash/GGBFS-based geopolymer mortar with load-induced damage, Mater. Struct. 53 (2020) 1–21.

[34] A. Fernandez-Jimenez, J.Y. Pastor, A. Martin, A. Palomo, High-temperature resistance in alkali-activated cement, J. Am. Ceram. Soc. 93 (2010) 3411–3417.

[35] P. Duan, C.J. Yan, W. Zhou, W.J. Luo, C.H. Shen, An investigation of the microstructure and durability of a fluidized bed fly ash-metakaolin geopolymer after heat and acid exposure, Mater. Des. 74 (2015) 125–137.

[36] H.Y. Zhang, V. Kodur, B. Wu, L. Cao, S.L. Qi, Comparative thermal and mechanical performance of geopolymers derived from metakaolin and fly ash, J. Mater. Civ. Eng. 28 (2016), 04015092.

[37] P. Rovnanik, P. Bayer, P. Rovnanikova, Characterization of alkali activated slag paste after exposure to high temperatures, Construct. Build. Mater. 47 (2013) 1479–1487.

[38] S.M. Park, J.G. Jang, N.K. Lee, H.K. Lee, Physicochemical properties of binder gel in alkali-activated fly ash/slag exposed to high temperatures, Cement Concr. Res. 89 (2016) 72–79.

[39] R. He, N. Dai, Z.J. Wang, Thermal and mechanical properties of geopolymers exposed to high temperature: a literature review, Adv. Civ. Eng. (2020) 2020.

[40] M.R. Bangi, T. Horiguchi, Pore pressure development in hybrid fibre-reinforced high strength concrete at elevated temperatures, Cement Concr. Res. 41 (2011) 1150–1156.

[41] S. Sanchayan, S.J. Foster, High temperature behaviour of hybrid steel-PVA fibre reinforced reactive powder concrete, Mater. Struct. 49 (2016) 769–782.

[42] O.E. Babalola, P.O. Awoyera, D.H. Le, L.M.B. Romero, A review of residual strength properties of normal and high strength concrete exposed to elevated temperatures: impact of materials modification on behaviour of concrete composite, Construct. Build. Mater. 296 (2021), 123448.

[43] A. Alhamad, S. Yehia, E. Lubloy, M. Elchalakani, Performance of different concrete types exposed to elevated temperatures: a review, Materials 15 (2022) 5032.

[44] M. Amran, S.S. Huang, S. Debbarma, R.S.M. Rashid, Fire resistance of geopolymer concrete: a critical review, Construct. Build. Mater. 324 (2022), 126722.

[45] Q.F. Song, M.Z. Guo, T.C. Ling, A review of elevated-temperature properties of alternative binders: supplementary cementitious materials and alkali-activated materials, Construct. Build. Mater. 341 (2022), 127894.

[46] Z.X. Wang, X. Rong, L. Zhao, X.Y. Xing, H. Ma, A review on fire-resistance performance of geopolymer coatings, Fresenius Environ. Bull. 31 (2022) 5357–5362.

[47] Y. Li, K.H. Tan, E.H. Yang, Synergistic effects of hybrid polypropylene and steel fibers on explosive spalling prevention of ultra-high performance concrete at elevated temperature, Cement Concr. Compos. 96 (2019) 174–181.

[48] V. Kodur, W. Khaliq, Effect of temperature on thermal properties of different types of high-strength concrete (vol 23, pg 793, 2011), J. Mater. Civ. Eng. 23 (2011), 1764-1764.

[49] ISO-834 Fire resistance tests-elements—elements of building construction, International Standard ISO 834 (1975).

[50] ASTM E119, 16a Standard Test Methods for Fire Tests of Building Construction and Materials, ASTM International, 2016.

[51] KSF 2257 Method of Fire Resistance Test for Elements of Building Construction Korean Industrial Standard, 2014.

[52] A. Jis, 1304 Method of Fire Resistance Test for Structural Parts of Buildings, Japanese Industrial Standard, 1982.

[53] B. Subiyanto Subyakto, T. Hata, S. Kawai, Evaluation of fire-retardant properties of edge-jointed lumber from tropical fast-growing woods using cone calorimetry and a standard fire test, J. Wood Sci. 49 (2003) 241–247.

[54] I.K. Kwon, Y.B. Kwon, Experimental study on the fire resistance of steel columns protected with fire boards, Int J Steel Struct 12 (2012) 25–35.

[55] S.H. Park, K.S. Chung, S.M. Choi, A study on failure prediction and design equation of concrete filled square steel tube columns under fire condition, Int J Steel Struct 7 (2007) 183–191.

[56] D.D. Yang, F.Q. Liu, S.S. Huang, H. Yang, ISO 834 standard fire test and mechanism analysis of square tubed-reinforced-concrete columns, J. Constr. Steel Res. 175 (2020), 106316.

[57] M. Ozawa, H. Morimoto, Effects of various fibres on high-temperature spalling in high-performance concrete, Construct. Build. Mater. 71 (2014) 83–92.

[58] Y.S. Heo, J.G. Sanjayan, C.G. Han, M.C. Han, Synergistic effect of combined fibers for spalling protection of concrete in fire, Cement Concr. Res. 40 (2010) 1547–1554.

[59] N. Yermak, P. Pliya, A.L. Beaucour, A. Simon, A. Noumowe, Influence of steel and/or polypropylene fibres on the behaviour of concrete at high temperature: spalling, transfer and mechanical properties, Construct. Build. Mater. 132 (2017) 240–250.

[60] Y.N. Ding, C. Zhang, M.L. Cao, Y.L. Zhang, C. Azevedo, Influence of different fibers on the change of pore pressure of self-consolidating concrete exposed to fire, Construct. Build. Mater. 113 (2016) 456–469.

[61] D.Y. Gao, D.M. Yan, X.Y. Li, Splitting strength of GGBFS concrete incorporating with steel fiber and polypropylene fiber after exposure to elevated temperatures, Fire Saf. J. 54 (2012) 67–73.

[62] P. Pliya, A.L. Beaucour, A. Noumowe, Contribution of cocktail of polypropylene and steel fibres in improving the behaviour of high strength concrete subjected to high temperature, Construct. Build. Mater. 25 (2011) 1926–1934.

[63] W. Khaliq, V. Kodur, Thermal and mechanical properties of fiber reinforced high performance self-consolidating concrete at elevated temperatures, Cement Concr. Res. 41 (2011) 1112–1122.

[64] C. Bing, J.Y. Liu, Residual strength of hybrid-fiber-reinforced high-strength concrete after exposure to high temperatures, Cement Concr. Res. 34 (2004) 1065–1069.

[65] D. Zhang, A. Dasari, K.H. Tan, On the mechanism of prevention of explosive spalling in ultra-high performance concrete with polymer fibers, Cement Concr. Res. 113 (2018) 169–177.

[66] M. Ezziane, L. Molez, R. Jauberthie, D. Rangeard, Heat exposure tests on various types of fibre mortar, Eur J Environ Civ En 15 (2011) 715–726.

[67] X.W. Liang, C.Q. Wu, Y.K. Yang, Z.X. Li, Experimental study on ultra-high performance concrete with high fire resistance under simultaneous effect of elevated temperature and impact loading, Cement Concr. Compos. 98 (2019) 29–38.

[68] A.A. Deshpande, D. Kumar, R. Ranade, Influence of high temperatures on the residual mechanical properties of a hybrid fiber-reinforced strain-hardening cementitious composite, Construct. Build. Mater. 208 (2019) 283–295.

[69] M.R. Bangi, T. Horiguchi, Effect of fibre type and geometry on maximum pore pressures in fibre-reinforced high strength concrete at elevated temperatures, Cement Concr. Res. 42 (2012) 459–466.

[70] J. Novak, A. Kohoutkova, Mechanical properties of concrete composites subject to elevated temperature, Fire Saf. J. 95 (2018) 66–76.

[71] C.S. Poon, Z.H. Shui, L. Lam, Compressive behavior of fiber reinforced high-performance concrete subjected to elevated temperatures, Cement Concr. Res. 34 (2004) 2215–2222.

[72] F. Aslani, B. Samali, Constitutive relationships for steel fibre reinforced concrete at elevated temperatures, Fire Technol. 50 (2014) 1249–1268.

[73] F. Aslani, B. Samali, High strength polypropylene fibre reinforcement concrete at high temperature, Fire Technol. 50 (2014) 1229–1247.

[74] F.U.A. Shaikh, A. Hosan, Mechanical properties of steel fibre reinforced geopolymer concretes at elevated temperatures, Construct. Build. Mater. 114 (2016) 15–28.

[75] A. Jameran, I.S. Ibrahim, S.H.S. Yazan, S.N.A.A. Rahim, Mechanical properties of steel-polypropylene fibre reinforced concrete under elevated temperature, Procedia Eng. 125 (2015) 818–824.

[76] P.S. Bhat, V. Chang, M. Li, Effect of elevated temperature on strain-hardening engineered cementitious composites, Construct. Build. Mater. 69 (2014) 370–380.

[77] J. Kim, G.P. Lee, D.Y. Moon, Evaluation of mechanical properties of steel-fibre-reinforced concrete exposed to high temperatures by double-punch test, Construct. Build. Mater. 79 (2015) 182–191.

[78] K. Watanabe, M.R. Bangi, T. Horiguchi, The effect of testing conditions (hot and residual) on fracture toughness of fiber reinforced high-strength concrete subjected to high temperatures, Cement Concr. Res. 51 (2013) 6–13.

[79] X. Luo, W. Sun, S.Y.N. Chan, Effect of heating and cooling regimes on residual strength and microstructure of normal strength and high-performance concrete, Cement Concr. Res. 30 (2000) 379–383.

[80] S.Q. Yang, T.C. Ling, C.S. Poon, High temperature performance of wet-mix and dry-mix mortars prepared with different contents and size gradings of glass aggregates: hot test and cold test, Cement Concr. Compos. 108 (2020), 103548.

[81] P. Bamonte, P.G. Gambarova, Thermal and mechanical properties at high temperature of a very high-strength durable concrete, J. Mater. Civ. Eng. 22 (2010) 545–555.

[82] P. Bamonte, P.G. Gambarova, A study on the mechanical properties of self-compacting concrete at high temperature and after cooling, Mater. Struct. 45 (2012) 1375–1387.

[83] B. Zhang, N. Bicanic, Fracture energy of high-performance concrete at high temperatures up to 450 degrees C: the effects of heating temperatures and testing conditions (hot and cold), Mag. Concr. Res. 58 (2006) 277–288.

[84] X. Jiang, R. Xiao, M.M. Zhang, W. Hu, Y. Bai, B.S. Huang, A laboratory investigation of steel to fly ash-based geopolymer paste bonding behavior after exposure to elevated temperatures, Construct. Build. Mater. 254 (2020), 119267.

[85] S. Ishak, H.S. Lee, J.K. Singh, M.A.M. Ariffin, N.H.A.S. Lim, H.M. Yang, Performance of fly ash geopolymer concrete incorporating bamboo ash at elevated temperature, Materials 12 (2019) 3404.

[86] F.U.A. Shaikh, Effect of cooling on the residual mechanical properties and cracking of plain and fibrous geopolymer concretes at elevated temperatures, Struct. Concr. 20 (2019) 1583–1595.

[87] O.G. Zhang, L. Li, T. Long, P.K. Sarker, X.S. Shi, G.C. Cai, Q.Y. Wang, The effect of ordinary portland cement substitution on the thermal stability of geopolymer concrete, Materials 12 (2019) 2501.

[88] F. Shaikh, S. Haque, Behaviour of carbon and basalt fibres reinforced fly ash geopolymer at elevated temperatures, Int J Concr Struct M 12 (2018) 1–12.

[89] M. Sivasakthi, R. Jeyalakshmi, N.P. Rajamane, R. Jose, Thermal and structural micro analysis of micro silica blended fly ash based geopolymer composites, J. Non-Cryst. Solids 499 (2018) 117–130.

[90] S. Luhar, S. Chaudhary, I. Luhar, Thermal resistance of fly ash based rubberized geopolymer concrete, J. Build. Eng. 19 (2018) 420–428.

[91] F. Shaikh, S. Haque, Effect of nano silica and fine silica sand on compressive strength of sodium and potassium activators synthesised fly ash geopolymer at elevated temperatures, Fire Mater. 42 (2018) 324–335.

[92] J.R.A. Goncalves, Y. Boluk, V. Bindiganavile, Crack growth resistance in fibre reinforced alkali-activated fly ash concrete exposed to extreme temperatures, Mater. Struct. 51 (2018) 1–10.

[93] G. Mathew, B. Joseph, Flexural behaviour of geopolymer concrete beams exposed to elevated temperatures, J. Build. Eng. 15 (2018) 311–317.

[94] M. Kaya, M. Uysal, K. Yilmaz, C.D. Atis, Behaviour of geopolymer mortars after exposure to elevated temperatures, Mater Sci-Medzg 24 (2018) 428–436.

[95] M.T. Junaid, O. Kayali, A. Khennane, Response of alkali activated low calcium fly-ash based geopolymer concrete under compressive load at elevated temperatures, Mater. Struct. 50 (2017) 1–10.

[96] A.M. Rashad, A.S. Ouda, An investigation on alkali-activated fly ash pastes modified with quartz powder subjected to elevated temperatures, Construct. Build. Mater. 122 (2016) 417–425.

[97] M.T. Junaid, A. Khennane, O. Kayali, Performance of fly ash based geopolymer concrete made using non-pelletized fly ash aggregates after exposure to high temperatures, Mater. Struct. 48 (2015) 3357–3365.

[98] F.U.A. Shaikh, V. Vimonsatit, Compressive strength of fly-ash-based geopolymer concrete at elevated temperatures, Fire Mater. 39 (2015) 174–188.

[99] P.K. Sarker, S. Kelly, Z.T. Yao, Effect of fire exposure on cracking, spalling and residual strength of fly ash geopolymer concrete, Mater. Des. 63 (2014) 584–592.

[100] M.T. Junaid, A. Khennane, O. Kayali, A. Sadaoui, D. Picard, M. Fafard, Aspects of the deformational behaviour of alkali activated fly ash concrete at elevated temperatures, Cement Concr. Res. 60 (2014) 24–29.

[101] O.A. Abdulkareem, A.M.M. Al Bakri, H. Kamarudin, I.K. Nizar, A.A. Saif, Effects of elevated temperatures on the thermal behavior and mechanical performance of fly ash geopolymer paste, mortar and lightweight concrete, Construct. Build. Mater. 50 (2014) 377–387.

[102] O.A. Abdulkareem, M.M.A. Abdullah, K. Hussin, K.N. Ismail, M. Binhussain, Mechanical and microstructural evaluations of lightweight aggregate geopolymer concrete before and after exposed to elevated temperatures, Materials 6 (2013) 4450–4461.

[103] S. Thokchom, K.K. Mandal, S. Ghosh, Effect of Si/Al ratio on performance of fly ash geopolymers at elevated temperature, Arabian J. Sci. Eng. 37 (2012) 977–989.

[104] Z. Pan, J.G. Sanjayan, Stress-strain behaviour and abrupt loss of stiffness of geopolymer at elevated temperatures, Cement Concr. Compos. 32 (2010) 657–664.

[105] D.L.Y. Kong, J.G. Sanjayan, Damage behavior of geopolymer composites exposed to elevated temperatures, Cement Concr. Compos. 30 (2008) 986–991.

[106] W.D.A. Rickard, C.S. Kealley, A. van Riessen, Thermally induced microstructural changes in fly ash geopolymers: experimental results and proposed model, J. Am. Ceram. Soc. 98 (2015) 929–939.

[107] S.N. Abd Razak, N. Shafiq, L. Guillaumat, S.A. Farhan, V.K. Lohana, Fire-exposed fly-ash-based geopolymer concrete: effects of burning temperature on mechanical and microstructural properties, Materials 15 (2022) 1884.

[108] S. Guler, Z.F. Akbulut, Effect of high-temperature on the behavior of single and hybrid glass and basalt fiber added cement mortars, J. Build. Eng. 57 (2022), 104809.

[109] M. Hanumananaik, M.S.K. Reddy, K.V.L. Subramaniam, High-temperature performance of low-calcium fly ash-based geopolymers, J. Mater. Civ. Eng. 34 (2022), 04022040.

[110] S.N.A. Razak, N. Shafiq, E.H. Nikbakht, B.S. Mohammed, L. Guillaumat, S. A. Farhan, Fire performance of fly-ash-based geopolymer concrete: effect of burning temperature on mechanical and microstructural properties, Mater. Today Proc. 66 (2022) 2665–2669.

[111] M. Kaya, Effect of steel fiber additive on high temperature resistance in geopolymer mortars, Ijst-T Civ Eng 46 (2022) 1949–1967.

[112] O. Topal, M.B. Karakoc, A. Ozcan, Effects of elevated temperatures on the properties of ground granulated blast furnace slag (GGBFS) based geopolymer concretes containing recycled concrete aggregate, Eur J Environ Civ En (2021) 4847–4862.

[113] S. Celikten, M. Saridemir, K. Akcaozoglu, Effect of calcined perlite content on elevated temperature behaviour of alkali activated slag mortars, J. Build. Eng. 32 (2020), 101717.

[114] I.H. Aziz, M.M.A. Abdullah, C.Y. Heah, Y.M. Liew, Behaviour changes of ground granulated blast furnace slag geopolymers at high temperature, Adv. Cement Res. 32 (2020) 465–475.

[115] R. Manjunath, M.C. Narasimhan, K.M. Umesha, Studies on high performance alkali activated slag concrete mixes subjected to aggressive environments and sustained elevated temperatures, Construct. Build. Mater. 229 (2019), 116887.

[116] K. Behfarnia, M. Shahbaz, The effect of elevated temperature on the residual tensile strength and physical properties of the alkali-activated slag concrete, J. Build. Eng. 20 (2018) 442–454.

[117] H.T. Turker, M. Balcikanli, I.H. Durmus, E. Ozbay, M. Erdemir, Microstructural alteration of alkali activated slag mortars depend on exposed high temperature level, Construct. Build. Mater. 104 (2016) 169–180.

[118] H.M. Khater, Studying the effect of thermal and acid exposure on alkali activated slag Geopolymer, International Congress on Materials & Structural Stability 11 (2014) 1–9.

[119] A.M. Rashad, S.R. Zeedan, A.A. Hassan, Influence of the activator concentration of sodium silicate on the thermal properties of alkali-activated slag pastes, Construct. Build. Mater. 102 (2016) 811–820.

[120] L. Zuda, Z. Pavlik, P. Rovnanikova, P. Bayer, R. Cerny, Properties of alkali activated aluminosilicate material after thermal load, Int. J. Thermophys. 27 (2006) 1250–1263.

[121] M. Guerrieri, J. Sanjayan, F. Collins, Residual compressive behavior of alkali-activated concrete exposed to elevated temperatures, Fire Mater. 33 (2009) 51–62.

[122] A.N. Derinpinar, M.B. Karakoc, A. Ozcan, Performance of glass powder substituted slag based geopolymer concretes under high temperature, Construct. Build. Mater. 331 (2022), 127318.

[123] A. Albidah, A. Abadel, F. Alrshoudi, A. Altheeb, H. Abbas, Y. Al-Salloum, Bond strength between concrete substrate and metakaolin geopolymer repair mortars at ambient and elevated temperatures, J. Mater. Res. Technol. 9 (2020) 10732–10745.

[124] M. Lahoti, K.K. Wong, E.H. Yang, K.H. Tan, Effects of Si/Al molar ratio on strength endurance and volume stability of metakaolin geopolymers subject to elevated temperature, Ceram. Int. 44 (2018) 5726–5734.

[125] P. Behera, V. Baheti, J. Militky, P. Louda, Elevated temperature properties of basalt microfibril filled geopolymer composites, Construct. Build. Mater. 163 (2018) 850–860.

[126] P. Behera, V. Baheti, J. Militky, S. Naeem, Microstructure and mechanical properties of carbon microfiber reinforced geopolymers at elevated temperatures, Construct. Build. Mater. 160 (2018) 733–743.

[127] K.M.L. Alventosa, B. Wild, C.E. White, The effects of calcium hydroxide and activator chemistry on alkali-activated metakaolin pastes exposed to high temperatures, Cement Concr. Res. 154 (2022), 106742.

[128] H.M. Khater, M. Gharieb, Synergetic effect of nano-silica fume for enhancing physico-mechanical properties and thermal behavior of MK-geopolymer composites, Construct. Build. Mater. 350 (2022), 128879.

[129] M. Saridemir, S. Celikten, Investigation of fire and chemical effects on the properties of alkali-activated lightweight concretes produced with basaltic pumice aggregate, Construct. Build. Mater. 260 (2020), 119969.

[130] K. Yasaswini, A.V. Rao, Behaviour of geopolymer concrete at elevated temperature, Mater. Today Proc. 33 (2020) 239–244.

[131] S. Celikten, M. Saridemir, I.O. Deneme, Mechanical and microstructural properties of alkali-activated slag and slag plus fly ash mortars exposed to high temperature, Construct. Build. Mater. 217 (2019) 50–61.

[132] S.J. Chithambaram, S. Kumar, M.M. Prasad, Thermo-mechanical characteristics of geopolymer mortar, Construct. Build. Mater. 213 (2019) 100–108.

[133] J.R. Ren, H.G. Chen, R.X. Dai, T. Sun, Behavior of combined fly ash/GBFS-based geopolymer concrete after exposed to elevated temperature, in: 2019 3rd International Workshop on Renewable Energy and Development (Iwred 2019), 267, 2019, 0323056.

[134] G.F. Huseien, A.R.M. Sam, J. Mirza, M.M. Tahir, M.A. Asaad, M. Ismail, K. W. Shah, Waste ceramic powder incorporated alkali activated mortars exposed to elevated Temperatures: performance evaluation, Construct. Build. Mater. 187 (2018) 307–317.

[135] W.G.V. Saavedra, R.M. de Gutierrez, Performance of geopolymer concrete composed of fly ash after exposure to elevated temperatures, Construct. Build. Mater. 154 (2017) 229–235.

[136] J.R. Ren, H.G. Chen, T. Sun, H. Song, M.S. Wang, Flexural behaviour of combined FA/GGBFS geopolymer concrete beams after exposure to elevated temperatures, Adv. Mater. Sci. Eng. 2017 (2017).

[137] G. Kurklu, The effect of high temperature on the design of blast furnace slag and coarse fly ash-based geopolymer mortar, Compos. B Eng. 92 (2016) 9–18.

[138] W.B. Ren, J.Y. Xu, E.L. Bai, Strength and ultrasonic characteristics of alkali-activated fly ash-slag geopolymer concrete after exposure to elevated temperatures, J. Mater. Civ. Eng. 28 (2016), 04015124.

[139] M. Guerrieri, J.G. Sanjayan, Behavior of combined fly ash/slag-based geopolymers when exposed to high temperatures, Fire Mater. 34 (2010) 163–175.

[140] J.B. Sundararaj, P.R.K. Rajkumar, M. Sivasakthi, M. Jegan, Effect of mineral admixtures on mechanical and thermal properties of geopolymer mortar at elevated temperature, Innov Infrastruct So 7 (2022) 1–14.

[141] S. Sasui, G. Kim, J. Nam, A. van Riessen, M. Hadzima-Nyarko, G. Choe, D. Suh, W. Jinwuth, Effects of waste glass sand on the thermal behavior and strength of fly ash and GGBS based alkali activated mortar exposed to elevated temperature, Construct. Build. Mater. 316 (2022), 125864.

[142] C.L. Chan, M.Z. Zhang, Behaviour of strain hardening geopolymer composites at elevated temperatures, Cement Concr. Compos. 132 (2022), 104634.

[143] H.Y. Zhang, G.H. Qiu, V. Kodur, Z.S. Yuan, Spalling behavior of metakaolin-fly ash based geopolymer concrete under elevated temperature exposure, Cement Concr. Compos. 106 (2020), 103483.

[144] H.Y. Zhang, V. Kodur, B. Wu, J. Yan, Z.S. Yuan, Effect of temperature on bond characteristics of geopolymer concrete, Construct. Build. Mater. 163 (2018) 277–285.

[145] H.Y. Zhang, V. Kodur, B. Wu, L. Cao, F. Wang, Thermal behavior and mechanical properties of geopolymer mortar after exposure to elevated temperatures, Construct. Build. Mater. 109 (2016) 17–24.

[146] P. Duan, C.J. Yan, W. Zhou, W.J. Luo, Thermal behavior of portland cement and fly ash-metakaolin-based geopolymer cement pastes, Arabian J. Sci. Eng. 40 (2015) 2261–2269.

[147] F. Ameri, P. Shoaei, S.A. Zareei, B. Behforouz, Geopolymers vs. alkali-activated materials (AAMs): a comparative study on durability, microstructure, and resistance to elevated temperatures of lightweight mortars, Construct. Build. Mater. 222 (2019) 49–63.

[148] Y.J. Zhang, S. Li, Y.C. Wang, D.L. Xu, Microstructural and strength evolutions of geopolymer composite reinforced by resin exposed to elevated temperature, J. Non-Cryst. Solids 358 (2012) 620–624.

[149] J.Y. Ye, W.S. Zhang, D. Shi, Effect of elevated temperature on the properties of geopolymer synthesized from calcined ore-dressing tailing of bauxite and ground-granulated blast furnace slag, Construct. Build. Mater. 69 (2014) 41–48.

[150] M.A. Salih, N. Farzadnia, R. Demirboga, A.A.A. Ali, Effect of elevated temperatures on mechanical and microstructural properties of alkali-activated mortar made up of POFA and GGBS, Construct. Build. Mater. 328 (2022), 127041.

[151] N. Ranjbar, M. Mehrali, U.J. Alengaram, H.S.C. Metselaar, M.Z. Jumaat, Compressive strength and microstructural analysis of fly ash/palm oil fuel ash based geopolymer mortar under elevated temperatures, Construct. Build. Mater. 65 (2014) 114–121.

[152] K.D. Hertz, Concrete strength for fire safety design, Mag. Concr. Res. 57 (2005) 445–453.

[153] A. Noumowe, Mechanical properties and microstructure of high strength concrete containing polypropylene fibres exposed to temperatures up to 200 degrees C, Cement Concr. Res. 35 (2005) 2192–2198.

[154] G.F. Peng, W.W. Yang, H. Zhao, Y.F. Liu, S.H. Bian, L.H. Zhao, Explosive spalling and residual mechanical properties of fiber-toughened high-performance concrete subjected to high temperatures, Cement Concr. Res. 36 (2006) 723–727.

[155] S.L. Suhaendi, T. Horiguchi, Effect of short fibers on residual permeability and mechanical properties of hybrid fibre reinforced high strength concrete after heat exposition, Cement Concr. Res. 36 (2006) 1672–1678.

[156] K.Y. Kim, T.S. Yun, K.P. Park, Evaluation of pore structures and cracking in cement paste exposed to elevated temperatures by X-ray computed tomography, Cement Concr. Res. 50 (2013) 34–40.

[157] Y. Li, in: Material Properties and Explosive Spalling of Ultra-high Performance Concrete in Fire. (Thesis), 2018, pp. 68–80.

[158] Z. Bažant, G. Cusatis, Concrete Creep at High Temperature and its Interaction with Fracture: Recent Progress, Creep, Shrinkage and Durability of Concrete and Concrete Structures, 2005.

[159] H.L. Zhang, C.T. Davie, A numerical investigation of the influence of pore pressures and thermally induced stresses for spalling of concrete exposed to elevated temperatures, Fire Saf. J. 59 (2013) 102–110.

[160] J. Zhao, J.J. Zheng, G.F. Peng, K. van Breugel, A meso-level investigation into the explosive spalling mechanism of high-performance concrete under fire exposure, Cement Concr. Res. 65 (2014) 64–75.

[161] E.W. Klingsch, Explosive spalling of concrete in fire, IBK Bericht (2014) 356.

[162] A. Behnood, M. Ghandehari, Comparison of compressive and splitting tensile strength of high-strength concrete with and without polypropylene fibers heated to high temperatures, Fire Saf. J. 44 (2009) 1015–1022.

[163] P. Duxson, A. Fernandez-Jimenez, J.L. Provis, G.C. Lukey, A. Palomo, J.S.J. van Deventer, Geopolymer technology: the current state of the art, J. Mater. Sci. 42 (2007) 2917–2933.

[164] R. Zhao, J.G. Sanjayan, Geopolymer and Portland cement concretes in simulated fire, Mag. Concr. Res. 63 (2011) 163–173.

[165] K. Traven, M. Cesnovar, S.D. Skapin, V. Ducman, High temperature resistant fly-ash and metakaolin-based alkali-activated foams, Ceram. Int. 47 (2021) 25105–25120.

[166] T. Bakharev, Geopolymeric materials prepared using Class F fly ash and elevated temperature curing, Cement Concr. Res. 35 (2005) 1224–1232.

[167] G.R. Consolazio, M. McVay, J. Rish III, Measurement and prediction of pore pressure in cement mortar subjected to elevated temperature, in: Proceedings of the International Workshop on Fire Performance of High-Strength Concrete, NIST, Gaithersburg, Maryland, 1997, pp. 125–148.

[168] H.L. Ye, A. Radlinska, Fly ash-slag interaction during alkaline activation: influence of activators on phase assemblage and microstructure formation, Construct. Build. Mater. 122 (2016) 594–606.

[169] I. Garcia-Lodeiro, A. Fernandez-Jimenez, A. Palomo, Variation in hybrid cements over time. Alkaline activation of fly ash-portland cement blends, Cement Concr. Res. 52 (2013) 112–122.

[170] S.F. Dai, L. Zhao, S.P. Peng, C.L. Chou, X.B. Wang, Y. Zhang, D. Li, Y.Y. Sun, Abundances and distribution of minerals and elements in high-alumina coal fly ash from the Jungar Power Plant, Inner Mongolia, China, Int. J. Coal Geol. 81 (2010) 320–332.

[171] H. Schneider, J. Schreuer, B. Hildmann, Structure and properties of mullite - a review, J. Eur. Ceram. Soc. 28 (2008) 329–344.

[172] N. Kawai, K.G. Nakamura, K. Kondo, High-pressure phase transition of mullite under shock compression, J. Appl. Phys. 96 (2004) 4126–4130.

[173] T. Sato, M. Ishizuka, M. Shimada, Sintering and characterization of mullite alumina composites, Ceram. Int. 12 (1986) 61–65.

[174] C. Aksel, The effect of mullite on the mechanical properties and thermal shock behaviour of alumina-mullite refractory materials, Ceram. Int. 29 (2003) 183–188.

[175] T. Alomayri, F.U.A. Shaikh, I.M. Low, Thermal and mechanical properties of cotton fabric-reinforced geopolymer composites, J. Mater. Sci. 48 (2013) 6746–6752.

[176] A. Martin, J.Y. Pastor, A. Palomo, A.F. Jimenez, Mechanical behaviour at high temperature of alkali-activated aluminosilicates (geopolymers), Construct. Build. Mater. 93 (2015) 1188–1196.

[177] A.M. Rashad, Y. Bai, P.A.M. Basheer, N.C. Collier, N.B. Milestone, Chemical and mechanical stability of sodium sulfate activated slag after exposure to elevated temperature, Cement Concr. Res. 42 (2012) 333–343.

[178] W.D.A. Rickard, L. Vickers, A. van Riessen, Performance of fibre reinforced, low density metakaolin geopolymers under simulated fire conditions, Appl. Clay Sci. 73 (2013) 71–77.

[179] N.K. Lee, K.T. Koh, G.H. An, G.S. Ryu, Influence of binder composition on the gel structure in alkali activated fly ash/slag pastes exposed to elevated temperatures, Ceram. Int. 43 (2017) 2471–2480.

[180] A.M.M. Al Bakri, H. Kamarudin, M. Bnhussain, A.R. Rafiza, Y. Zarina, Effect of Na2SiO3/NaOH ratios and NaOH molarities on compressive strength of fly-ash-based geopolymer, ACI Mater. J. 109 (2012) 503–508.

[181] A. Fernandez-Jimenez, A. Palomo, J.Y. Pastor, A. Martin, New cementitious materials based on alkali-activated fly ash: performance at high temperatures, J. Am. Ceram. Soc. 91 (2008) 3308–3314.

[182] W.D.A. Rickard, J. Temuujin, A. van Riessen, Thermal analysis of geopolymer pastes synthesised from five fly ashes of variable composition, J. Non-Cryst. Solids 358 (2012) 1830–1839.

[183] R.P. Williams, R.D. Hart, A. van Riessen, Quantification of the extent of reaction of metakaolin-based geopolymers using X-ray diffraction, scanning electron microscopy, and energy-dispersive spectroscopy, J. Am. Ceram. Soc. 94 (2011) 2663–2670.

[184] H. Cheng-Yong, L. Yun-Ming, M.M.A. Abdullah, K. Hussin, Thermal resistance variations of fly ash geopolymers: foaming responses, Sci Rep-Uk 7 (2017) 1–11.

[185] T. Bakharev, Thermal behaviour of geopolymers prepared using class F fly ash and elevated temperature curing, Cement Concr. Res. 36 (2006) 1134–1147.

[186] N.Y. Mostafa, Q. Mohsen, A. El-maghraby, Characterization of low-purity clays for geopolymer binder formulation, Int J Min Met Mater 21 (2014) 609–619.

[187] M. Lahoti, K.K. Wong, K.H. Tan, E.H. Yang, Effect of alkali cation type on strength endurance of fly ash geopolymers subject to high temperature exposure, Mater. Des. 154 (2018) 8–19.

[188] W.R.A.V. Riessen, J. Sanjayan, Geopolymers: Structure, Processing, Properties and Industrial Applications, Woodhead Publ Mater, 2009, pp. 1–454.

[189] W.D.A. Rickard, A. van Riessen, Performance of solid and cellular structured fly ash geopolymers exposed to a simulated fire, Cement Concr. Compos. 48 (2014) 75–82.

[190] I. Ismail, S.A. Bernal, J.L. Provis, R.S. Nicolas, S. Hamdan, J.S.J. van Deventer, Modification of phase evolution in alkali-activated blast furnace slag by the incorporation of fly ash, Cement Concr. Compos. 45 (2014) 125–135.

[191] S.A. Bernal, J.L. Provis, B. Walkley, R.S. Nicolas, J.D. Gehman, D.G. Brice, A.R. Kilcullen, P. Duxson, J.S.J. van Deventer, Gel nanostructure in alkali-activated binders based on slag and fly ash, and effects of accelerated carbonation, Cement Concr. Res. 53 (2013) 127–144.

[192] S.A. Bernal, J.L. Provis, Durability of alkali- activated materials: progress and perspectives, J. Am. Ceram. Soc. 97 (2014) 997–1008.

[193] I. Garcia-Lodeiro, A. Palomo, A. Fernandez-Jimenez, D.E. Macphee, Compatibility studies between N-A-S-H and C-A-S-H gels. Study in the ternary diagram Na2O-CaO-Al2O3-SiO2-H2O, Cement Concr. Res. 41 (2011) 923–931.

[194] K. Dombrowski, A. Buchwald, M. Weil, The influence of calcium content on the structure and thermal performance of fly ash based geopolymers, J. Mater. Sci. 42 (2007) 3033–3043.

[195] Y.M. Gu, Y.H. Fang, D. You, Y.F. Gong, C.H. Zhu, Properties and microstructure of alkali-activated slag cement cured at below- and about-normal temperature, Construct. Build. Mater. 79 (2015) 1–8.

[196] M.M. Salahuddin, M. Norkhairunnisa, F. Mustapha, A review on thermophysical evaluation of alkali-activated geopolymers, Ceram. Int. 41 (2015) 4273–4281.

[197] H. Rahier, B. VanMele, M. Biesemans, J. Wastiels, X. Wu, Low-temperature synthesized aluminosilicate glasses .1. Low-temperature reaction stoichiometry and structure of a model compound, J. Mater. Sci. 31 (1996) 71–79.

[198] W.D.A. Rickard, A. van Riessen, P. Walls, Thermal character of geopolymers synthesized from class F fly ash containing high concentrations of iron and alpha-quartz, Int. J. Appl. Ceram. Technol. 7 (2010) 81–88.

[199] W.D.A. Rickard, G.J.G. Gluth, K. Pistol, In-situ thermo-mechanical testing of fly ash geopolymer concretes made with quartz and expanded clay aggregates, Cement Concr. Res. 80 (2016) 33–43.

[200] L. Carabba, R. Moricone, G.E. Scarponi, A. Tugnoli, M.C. Bignozzi, Alkali activated lightweight mortars for passive fire protection: a preliminary study, Construct. Build. Mater. 195 (2019) 75–84.

[201] I.J. Merchant, D.E. Macphee, H.W. Chandler, R.J. Henderson, Toughening cement-based materials through the control of interfacial bonding, Cement Concr. Res. 31 (2001) 1873–1880.

[202] L. Vickers, W.D.A. Rickard, A. van Riessen, Strategies to control the high temperature shrinkage of fly ash based geopolymers, Thermochim. Acta 580 (2014) 20–27.

[203] D.L.Y. Kong, J.G. Sanjayan, K. Sagoe-Crentsil, Factors affecting the performance of metakaolin geopolymers exposed to elevated temperatures, J. Mater. Sci. 43 (2008) 824–831.

[204] K.M. Klima, K. Schollbach, H.J.H. Brouwers, Q.L. Yu, Thermal and fire resistance of Class F fly ash based geopolymers-A review, Construct. Build. Mater. 323 (2022) 126529.

[205] K. Kupwade-Patil, F. Soto, A. Kunjumon, E.N. Allouche, D.S. Mainardi, Multi-scale modeling and experimental investigations of geopolymeric gels at elevated temperatures, Comput. Struct. 122 (2013) 164–177.

[206] T. Kovarik, D. Rieger, J. Kadlec, T. Krenek, L. Kullova, M. Pola, P. Belsky, P. France, J. Riha, Thermomechanical properties of particle-reinforced geopolymer composite with various aggregate gradation of fine ceramic filler, Construct. Build. Mater. 143 (2017) 599–606.

[207] A. Behnood, H. Ziari, Effects of silica fume addition and water to cement ratio on the properties of high-strength concrete after exposure to high temperatures, Cement Concr. Compos. 30 (2008) 106–112.

[208] J.H. Xie, Z. Zhang, Z.Y. Lu, M.W. Sun, Coupling effects of silica fume and steel-fiber on the compressive behaviour of recycled aggregate concrete after exposure to elevated temperature, Construct. Build. Mater. 184 (2018) 752–764.

[209] B. Georgali, P.E. Tsakiridis, Microstructure of fire-damaged concrete. A case study, Cement Concr. Compos. 27 (2005) 255–259.

[210] V.K.R. Kodur, M.A. Sultan, Effect of temperature on thermal properties of high-strength concrete, J. Mater. Civ. Eng. 15 (2003) 101–107.

[211] S.M.M. Alizadeh, A. Rezaeian, I. Rasoolan, B. Tahmouresi, Compressive stress-strain model and residual strength of self-compacting concrete containing recycled ceramic aggregate after exposure to fire, J. Build. Eng. 38 (2021), 102206.

[212] Y.C. Guo, J.H. Zhang, G.M. Chen, Z.H. Xie, Compressive behaviour of concrete structures incorporating recycled concrete aggregates, rubber crumb and reinforced with steel fibre, subjected to elevated temperatures, J. Clean. Prod. 72 (2014) 193–203.

[213] T.C. Ling, C.S. Poon, S.C. Kou, Influence of recycled glass content and curing conditions on the properties of self-compacting concrete after exposure to elevated temperatures, Cement Concr. Compos. 34 (2012) 265–272.

[214] B. Arisoy, H.C. Wu, Material characteristics of high performance lightweight concrete reinforced with PVA, Construct. Build. Mater. 22 (2008) 635–645.

[215] K. Schneider, A. Michel, M. Liebscher, L. Terreri, S. Hempel, V. Mechtcherine, Mineral-impregnated carbon fibre reinforcement for high temperature resistance of thin-walled concrete structures, Cement Concr. Compos. 97 (2019) 68–77.

[216] A.B. Kizilkanat, N. Kabay, V. Akyuncu, S. Chowdhury, A.R. Akca, Mechanical properties and fracture behavior of basalt and glass fiber reinforced concrete: an experimental study, Construct. Build. Mater. 100 (2015) 218–224.

[217] Z.G. Zhang, Q. Zhang, Matrix tailoring of Engineered Cementitious Composites (ECC) with non-oil-coated, low tensile strength PVA fiber, Construct. Build. Mater. 161 (2018) 420–431.

[218] J.C. Liu, K.H. Tan, Mechanism of PVA fibers in mitigating explosive spalling of engineered cementitious composite at elevated temperature, Cement Concrete Comp 93 (2018) 235–245.

[219] M.M. Hilles, M.M. Ziara, Mechanical behavior of high strength concrete reinforced with glass fiber, Eng Sci Technol 22 (2019) 920–928.

[220] S. Liu, D.J. Zhu, Y.F. Ou, Y.M. Yao, C.J. Shi, Impact response of basalt textile reinforced concrete subjected to different velocities and temperatures, Constr Build Mater 175 (2018) 381–391.

[221] H.R. Pakravan, M. Latifi, M. Jamshidi, Hybrid short fiber reinforcement system in concrete: a review, Constr Build Mater 142 (2017) 280–294.

[222] Z. Wang, J.Z. Ju, J.S. Yang, Z. Ma, D. Liu, K.P. Cui, H.R. Yang, J.R. Chang, N. D. Huang, L.B. Li, The non-equilibrium phase diagrams of flow-induced crystallization and melting of polyethylene, Sci Rep-Uk 6 (2016) 1–8.

[223] M. Kalaj, M.S. Denny, K.C. Bentz, J.M. Palomba, S.M. Cohen, Nylon-MOF composites through postsynthetic polymerization, Angew Chem Int Edit 58 (2019) 2336–2340.

[224] N. Ranjbar, M.Z. Zhang, Fiber-reinforced geopolymer composites: a review, Cement Concrete Comp 107 (2020), 103498.

[225] J.D. Rios, C. Leiva, M.P. Ariza, S. Seitl, H. Cifuentes, Analysis of the tensile fracture properties of ultra-high-strength fiber-reinforced concrete with different types of steel fibers by X-ray tomography, Mater Design 165 (2019), 107582.

[226] W.Z. Zheng, B.F. Luo, Y. Wang, Compressive and tensile properties of reactive powder concrete with steel fibres at elevated temperatures, Constr Build Mater 41 (2013) 844–851.

[227] W.Z. Zheng, H.Y. Li, Y. Wang, Compressive stress-strain relationship of steel fiber-reinforced reactive powder concrete after exposure to elevated temperatures, Constr Build Mater 35 (2012) 931–940.

[228] W.Z. Zheng, B.F. Luo, Y. Wang, Stress-strain relationship of steel-fibre reinforced reactive powder concrete at elevated temperatures, Mater Struct 48 (2015) 2299–2314.

[229] F. Aslani, J. Kelin, Assessment and development of high-performance fibre-reinforced lightweight self-compacting concrete including recycled crumb rubber aggregates exposed to elevated temperatures, J Clean Prod 200 (2018) 1009–1025.

[230] L.H. Xu, L. Huang, Y. Chi, G.D. Mei, Tensile behavior of steel-polypropylene hybrid fiber-reinforced concrete, Aci Mater J 113 (2016) 219–229.

[231] Y.N. Chan, X. Luo, W. Sun, Compressive strength and pore structure of high-performance concrete after exposure to high temperature up to 800 degrees C, Cement Concrete Res 30 (2000) 247–251.

[232] K.K. Sideris, P. Manita, E. Chaniotakis, Performance of thermally damaged fibre reinforced concretes, Constr Build Mater 23 (2009) 1232–1239.

[233] Y.S. Heo, J.G. Sanjayan, C.G. Han, M.C. Han, Critical parameters of nylon and other fibres for spalling protection of high strength concrete in fire, Mater Struct 44 (2011) 599–610.

[234] C.G. Han, Y.S. Hwang, S.H. Yang, N. Gowripalan, Performance of spalling resistance of high performance concrete with polypropylene fiber contents and lateral confinement, Cement Concrete Res 35 (2005) 1747–1753.

[235] A.N.S.A.L. Qadi, K.N. Bin Mustapha, S. Naganathan, Q.N.S. Al-Kadi, Effect of polypropylene fibers on thermogravimetric properties of self-compacting concrete at elevated temperatures, Fire Mater 37 (2013) 177–186.

[236] W. Khaliq, V. Kodur, High temperature mechanical properties of high-strength fly ash concrete with and without fibers, Aci Mater J 109 (2012) 665–674.

[237] W.Z. Zheng, H.Y. Li, Y. Wang, Compressive behaviour of hybrid fiber-reinforced reactive powder concrete after high temperature, Mater Design 41 (2012) 403–409.

[238] R. Serrano, A. Cobo, M.I. Prieto, M.D. Gonzalez, Analysis of fire resistance of concrete with polypropylene or steel fibers, Constr Build Mater 122 (2016) 302–309.

[239] V.M.D. Monteiro, L.R. Lima, F.D. Silva, On the mechanical behavior of polypropylene, steel and hybrid fiber reinforced self-consolidating concrete, Constr Build Mater 188 (2018) 280–291.

[240] J. Eidan, I. Rasoolan, A. Rezaeian, D. Poorveis, Residual mechanical properties of polypropylene fiber-reinforced concrete after heating, Constr Build Mater 198 (2019) 195–206.

[241] P.N. Hiremath, S.C. Yaragal, Performance evaluation of reactive powder concrete with polypropylene fibers at elevated temperatures, Constr Build Mater 169 (2018) 499–512.